

Properties of Laser Ablation Products of Delrin with CO₂ Laser

EOARD Grant
Cooperative Agreement Award No. FA8655-03-1-3061

Final Report
May 2004



Project officer: Wolfgang O. Schall

Co-authors: Hans-Albert Eckel, Jochen Tegel, Frank Waiblinger,
Sebastian Walther

DLR – German Aerospace Center
Institute of Technical Physics
Pfaffenwaldring 38 – 40
D-70569 Stuttgart
Germany

Report Documentation Page

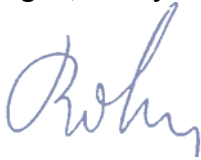
*Form Approved
OMB No. 0704-0188*

Public reporting burden for the collection of information is estimated to average 1 hour per response, including the time for reviewing instructions, searching existing data sources, gathering and maintaining the data needed, and completing and reviewing the collection of information. Send comments regarding this burden estimate or any other aspect of this collection of information, including suggestions for reducing this burden, to Washington Headquarters Services, Directorate for Information Operations and Reports, 1215 Jefferson Davis Highway, Suite 1204, Arlington VA 22202-4302. Respondents should be aware that notwithstanding any other provision of law, no person shall be subject to a penalty for failing to comply with a collection of information if it does not display a currently valid OMB control number.

1. REPORT DATE 00 JUL 2004	2. REPORT TYPE N/A	3. DATES COVERED -			
4. TITLE AND SUBTITLE Properties of Laser Ablation Products of Delrin with CO2 Laser		5a. CONTRACT NUMBER			
		5b. GRANT NUMBER			
		5c. PROGRAM ELEMENT NUMBER			
6. AUTHOR(S)		5d. PROJECT NUMBER			
		5e. TASK NUMBER			
		5f. WORK UNIT NUMBER			
7. PERFORMING ORGANIZATION NAME(S) AND ADDRESS(ES) DLR German Aerospace Center Institute of Technical Physics Pfaffenwaldring 38 40 D-70569 Stuttgart Germany		8. PERFORMING ORGANIZATION REPORT NUMBER			
		10. SPONSOR/MONITOR'S ACRONYM(S)			
9. SPONSORING/MONITORING AGENCY NAME(S) AND ADDRESS(ES)		11. SPONSOR/MONITOR'S REPORT NUMBER(S)			
		12. DISTRIBUTION/AVAILABILITY STATEMENT Approved for public release, distribution unlimited			
13. SUPPLEMENTARY NOTES See also ADM001699, EOARD-SPC 03-3061., The original document contains color images.					
14. ABSTRACT					
15. SUBJECT TERMS					
16. SECURITY CLASSIFICATION OF:			17. LIMITATION OF ABSTRACT SAR	18. NUMBER OF PAGES 78	19a. NAME OF RESPONSIBLE PERSON
a. REPORT unclassified	b. ABSTRACT unclassified	c. THIS PAGE unclassified			

The contractor, German Aerospace Center (DLR), Institute of Technical Physics, hereby declares that, to the best of its knowledge and belief, the technical data delivered herewith under Contract No: FA8655-03-1-3061 is complete, accurate, and complies with all requirements of the contract.

Stuttgart, May 2004



Prof. W. L. Bohn
Director
Institute of Technical Physics

I certify that there were no subject inventions to declare as defined in FAR 52.227-13, during the performance of this contract.

Stuttgart, May 2004



Prof. W. L. Bohn
Director
Institute of Technical Physics

SUMMARY

Properties of Laser Ablation Products of Delrin with CO₂ Laser

A requirement for efficient pulsed laser propulsion from ground to LEO is the achievement of a specific impulse of up to 800 s at a jet efficiency of at least 50%. With classical polymers like Delrin or POM these numbers cannot be obtained. The suggestion to use polymers with included metal powder for a better deposition of the laser energy per unit volume and thus the achievement of a higher jet velocity together with a lower ablation rate has been experimentally investigated. Samples of different polymers and different metal contents (Al and Mg in the range of 3% to 60% by weight) have been formulated and irradiated with CO₂ laser pulses of about 12 μ s in duration and energies of 40 J to 280 J (fluences of 20 to 150 J/cm²). The samples were mounted to a pendulum for measuring the exerted impulse and the mass loss per pulse was determined by weighing. These experiments have been carried out in ambient atmosphere, as well as at various pressure levels down to vacuum of less than 1 mbar in a vessel. In general, the expansion of the ablated material (vapor) was forced to be one-dimensional by applying a guiding tube. But three-dimensional expansions were investigated as well. Furthermore, the efficacy of certain selected formulations as a propellant have been tested in a bell shaped light concentrating structure. The samples have been inspected under an electron microscope before and after the laser interaction. Because a suspicion existed from the beginning of the experiments that a certain amount of the incident laser energy might be absorbed in a decoupled plasma wave (breakdown), time resolved power measurements of the incident energy, of the reflected energy from the target and, at a later stage, of the energy transmitted through a hole in the target were made.

The results did not fulfill the expectations. In air a major problem is the unknown amount of mass that participates in the acceleration of the ejected material and therefore all quantities that are related to the ablated mass only, in particular jet velocity and efficiency, yield too high numbers. These quantities are correct in vacuum, when only the ablated material is accelerated. Although the ablated mass is reduced indeed for metal doped polymers in comparison to the plain material, this does not result in a better performance, neither when

ablated from a flat surface, nor when irradiated in the bell type nozzle as in previous experiments. The measurements of the time dependent power transmitted through a hole in the sample has shown, that depending on the pulse energy a rather large fraction does not arrive at the target surface and is most likely absorbed in a decoupled vapor or plasma wave. The inspection of the irradiated samples document, that the imbedded metal grains at least have reached the melting temperature. But it remains doubtful, whether they are also vaporized or only ejected as dust. If the desire exists to improve the situation, an investigation of the absorption wave characteristics is inevitable.

Properties of Laser Ablation Products of Delrin with CO₂ Laser

1. Introduction

- 1.1 Purpose of the experiments
- 1.2 Background
- 1.3 Technical approach and methodology

2. Experimental setup and instrumentation

3. Formulation, acquisition and preparation of target samples

- 3.1 Sample types
- 3.2 Sample analysis under the electron microscope

4. Experimental results and interpretation

- 4.1 Measurements in air
- 4.2 3-D effects
- 4.3 Measurements at reduced ambient pressure and in vacuum
- 4.4 Comparison of different sample formulations
- 4.5 Time resolved power measurements
- 4.6 Tests with doped material in a light concentrating structure
- 4.7 Inspection of used samples by electron micrography

5. Conclusion and recommendations

Literature

Appendices

LIST OF FIGURES AND DIAGRAMS

Front page: Lightcraft flames in Alcohol (left) and titanium doped POM (right)

Fig. 1. Experimental setup

Fig. 2. Sketch of the optical arrangement

Fig. 3. Mirror Arrangement

Fig. 4. Laser pulse time profile

Fig. 5. Sketch of the sample holder with guiding tube

Fig. 6. Photograph of the sample holder in closed and open position

Fig. 7. Target sample

Fig. 8. Effect of several laser shots on Epoxy samples with 50% Al and 40% Mg

4.1 Measurements in air

Diagram 1 Shot to shot reproducibility of the impulse

Diagram 2 Ablated mass vs. pulse energy

Diagram 3 Upper limit of deposited energy vs. pulse energy

Diagram 4 Measured impulse vs. pulse energy

Diagram 5 Impulse data scatter of individual shots vs. pulse energy

Diagram 6 Coupling coefficient vs. pulse energy

Diagram 7 Limiting values of the exhaust velocities vs. pulse energy

Diagram 8 Limiting values of the jet efficiency vs. pulse energy

4.2 3-D effects

Diagram 9 Mass loss comparison

Diagram 10 Impulse comparison

Diagram 11 Exhaust velocity comparison

4.3 Measurements at reduced ambient pressure and in vacuum

Diagram 12 Ablated mass per pulse at a pulse energy of 280 J vs. pressure

Diagram 13 Ablated mass for Al doped POM vs. pressure

- Diagram 14** Apparent deposited energy vs. pressure
- Diagram 15** Coupling coefficient vs. pressure
- Diagram 16** Apparent exhaust velocity vs. pressure
- Diagram 17** Apparent jet efficiency vs. pressure
- Diagram 18** Ablated mass vs. pulse energy
- Diagram 19** Apparent deposited energy vs. pulse energy
- Diagram 20** Coupling coefficient vs. pulse energy
- Diagram 21** Apparent jet velocity vs. pulse energy
- Diagram 22** Apparent jet efficiency vs. pulse energy

4.4 Comparison of different sample formulations

- Diagram 23** Ablated mass
- Diagram 24** Deposited energy
- Diagram 25** Coupling coefficient
- Diagram 26** Jet velocity
- Diagram 27** Jet efficiency

4.5 Time resolved power measurements

- Diagram 28** Laser pulse on undoped POM with an energy of 200 J
- Diagram 29** Laser pulse on POM + 40% Al with an energy of 200 J
- Diagram 30** Power signals for pulses with 200 J and 280 J and target removed
- Diagram 31** Time resolved signals of incident, reflected and transmitted laser power
- Diagram 32** Pulse duration shortening effect with incident pulse energy

4.6 Tests with doped material in a light concentrating structure

- Diagram 33** Mass loss
- Diagram 34** Apparently deposited energy
- Diagram 35** Measured impulse
- Diagram 36** Coupling coefficient
- Diagram 37** Apparent exhaust velocity

Diagram 38 Apparent jet efficiency

1. INTRODUCTION

1.1 Purpose of the project

Purpose of the project is to develop an understanding of the parameters that control the specific energy (e.g. temperature) of gases that are produced by ablation of specially prepared samples of solid polymer materials (e.g. Delrin) with a pulsed CO₂ laser. The ablation materials will incorporate controlled amounts of metallic dopants for increased deposition of laser pulse energy. A target specific energy content of ≥ 100 MJ/kg for the ablated gas is desirable. The measurements will be carried out for flat plates and inside a parabolic light concentrating structure in air, at reduced pressure and in vacuum. Additionally desired target gas properties are a specific impulse range from 200 to 800 seconds, and an overall conversion efficiency of laser energy to jet kinetic energy of at least 50%.

1.2 Background

The experiments are a natural continuation of previous experiments run by Avco Research Laboratory Inc. from 1987 to 1991 (Ref. 1) with a special emphasis on the so-called Double Pulse Rocket Concept and of the measurements by DLR in 2000 and 2002 (Ref. 2 and 3). The principle of the double pulse concept is to apply a first pulse (ablation pulse) to evaporate a thin layer of the surface of a solid propellant. After a sufficient time gap to allow the vapor to expand over a characteristic distance of a centimeter, a second pulse with higher intensity (thrust pulse) is applied to generate a plasma via Inverse Bremsstrahlung and an associated detonation wave that produces the major part of the thrust. CO₂ lasers were expected to be especially suitable due to their long wavelength and high energy capabilities. When using polymers, such as polyacetal (brand name Delrin) it was noticed that the absorption length was too large and too much material was actually evaporated. In consequence, high thrust could be produced but with insufficient specific impulse. An attempt had been made to dope the target with metallic particles to enhance the surface absorption and therefore increase the amount of deposable energy per unit mass (ref. 1). Associated with this increase should be an increase in specific impulse due to less expended mass but at a higher exhaust velocity. Another necessary condition was the ionization of the gas with a leading pulse spike in a

time much shorter than the actual thrust length. Metallic powder with grain sizes in the order of the incident radiation wavelength would serve as dipole antennas that produce large currents in the electromagnetic field of the laser beam and subsequently vaporize in an extremely short time. Some experiments, preceding those in ref. 1, with doped material (Celcon with sodium valerate and trigger flakes) however failed to demonstrate a difference in deposited energy for single and double pulse experiments. This had been attributed to some evidence that the dispersal time of the propellant was much longer (several microseconds) than the time lag for the arrival of the thrust pulse (several hundred nanoseconds), so that this pulse could not find sufficient material for sustaining a detonation wave.

In subsequent experiments in ref. 1, measurements of the coupling coefficient and the velocity of the ablation products in vacuum were made, both with single and with double pulses. For single pulse measurements the spot size was varied to cover a fluence range from 2 J/cm^2 to 7 J/cm^2 . It is interesting to mention that the authors found no difference in behavior for plain Celcon targets and such with Al flakes and sodium valerate. The derived velocities in vacuum were around 1.8 km/s , independent of the fluence above 3 J/cm^2 . Although there is quite a large scattering in the data for the double pulse arrangement, a certain improvement in coupling and velocity with increasing thrust fluence (between 10 J/cm^2 and 30 J/cm^2) can be noticed, resulting in velocities $> 2 \text{ km/s}$. This improvement is attributed to a better absorption efficiency in the vapor produced by the precursor ablation pulse. Optimum time delay between the two pulses is around $4 - 5 \text{ } \mu\text{s}$.

In ref. 2 and 3 experiments are described that used plain Delrin as solid propellant, placed inside light concentrating structures, as are foreseen for laser propulsion. $10 - 12 \text{ } \mu\text{s}$ long pulses from a CO_2 laser were irradiated into the structure and the exerted impulse was measured in air at various pressures, and in vacuum at $p < 1 \text{ mbar}$. In addition, the mass loss per pulsed was determined. The coupling coefficient depended on the size of the propellant cylinder, indicating a dependence on the incident intensity and fluence at the propellant surface. At best, the coupling coefficient was independent on the pulse energy. In other cases it decreased with increasing pulse energy. Likewise, the exhaust velocity depended only very little on the pulse energy with a maximum of 2.5 km/s . The maximum energy deposition was 5.5 MJ/kg and was found for the lowest applied pulse energy of 120 J . The

behavior is an indication that a substantial and increasing fraction of the incident energy did not reach the target surface and was absorbed in a decoupled wave that did not contribute to the impulse generation. Whether this wave had the characteristics of a detonation wave or a slower laser combustion wave could not be discerned. In any case, the impulse was driven by the ablated mass and not by the velocity of the ablated expanding material. This raised the question how more energy could be deposited in the propellant.

1.3 Technical approach and methodology

As suggested by ref. 1, the absorption depth of infrared radiation in a solid polymer formulation may be reduced to an arbitrarily small value by increasing the dipole strength of the polymer with a small concentration of metal dopant. The amount of polymer, ablated by a laser pulse of given energy, and the specific energy content of ablated gases may be controlled by adjusting the quantity of fine metal powders, fibers and/or spheres that are embedded in the polymer. The best candidate polymer is one that is easily atomized to a low molecular weight gas but is not easily ionized. Fully atomized Delrin [or polyformaldehyde, $(\text{H}_2\text{CO})_n$] has a molecular weight of 7.5 g/mol. The best metal dopant is one that will, in small concentration, produce large effective dipole strength, e.g., silver, iron, and the light alkali metals, lithium or sodium.

When a properly doped polymer absorbs an impulse of laser energy, a high velocity jet normal to the polymer surface is produced. Jet properties may be measured and quantified in terms of (1) specific internal energy of ablated polymer (energy per unit mass), (2) specific impulse of the jet (impulse per unit mass of ablated polymer), (3) coupling coefficient (impulse of jet per unit laser energy), and (4) overall energy conversion efficiency (jet kinetic energy per unit laser energy). Measurement of the laser energy with a calorimeter, the ablated polymer mass by weighing before and after ablation, and the jet impulse with a ballistic pendulum, allows the overall efficiency of conversion of laser energy to jet kinetic energy, the specific impulse, and the coupling coefficient to be extracted (Refs. 2-7).

Ablation experiments with measurement of ablated mass, impulse, and laser energy need be carried out using selected polymer/metal dopant formulations with appropriate geometries that provide a reasonable expansion ratio of around 15 for good internal energy to jet kinetic energy conversion

(e.g., around 40% to 50%). An open paraboloidal cavity with polymer placed near the focus is one geometry that is easily subjected to thermodynamic idealization that enables establishment of an upper energy conversion limit based on isentropic expansion. The selected polymer formulations will need to have good mechanical strength and must produce clean ablation without fragmentation when subjected to laser pulse intensities in the range of 5 to 10 MW/cm², with fluence around 5 to 50 J/cm² and laser pulse widths ranging from 0.1 to 10 microseconds. Shorter pulse widths enable energy deposition into the polymer before gas expansion begins. Thus the heated polymer may be confined by its own inertia so that hot gas at densities near that of the solid are produced, around 1500 kg/m³, which translates to effective combustion chamber pressures of around 1,000 bar.

In order to achieve the intended goals the following tasks have been planned and carried out to the extent of technical and physical possibilities and constraints:

- Investigation of the formulation of different materials (i.e., delrin, epoxy, butadiene, etc.) and evaluation of alternative processes for the doping with metal powders in various concentrations; check for commercially available material mixtures; characterization of targets' physical properties in terms of density, dopant, particle distribution, etc.
- Experimental investigation of the ablation properties of different materials (polymers with metal powder in different concentrations) in order to decrease the mass of ablated material per pulse (volume absorption → surface absorption). Conduction of ablation experiments using flat plates over a range of laser intensities and fluence values that are experimentally accessible and considered most relevant. Determination of the values of ablated mass, specific energy, impulse, and coupling coefficient of the gas in aerial environment, at reduced pressure and in vacuum. Calculations will be made to define the exhaust velocity, specific impulse, and the efficiency of converting laser energy to propellant energy for each of the propellant formulations over a range of laser operating conditions.
- Measurement of coupling coefficient and ablated material mass of samples embodied inside a parabolic light concentrating structure in air, at reduced pressure and in vacuum.

- Promising sample formulations may be fabricated in a ring shape for testing and delivered to the AFRL's Propulsion Directorate at Edwards AFB on request.

2. EXPERIMENTAL SETUP AND INSTRUMENTATION

CO₂ laser, pendulum test stand, vacuum chamber and the diode laser based range finder, together with the PC based data acquisition system comprise the fundamental equipment for all the experiments. These items have been described in Ref. 3 in detail. For all the experiments the laser was run with a stable resonator. For geometrical reasons, the maximum achievable laser pulse energy is somewhat lower with this resonator than with an unstable resonator. On the other hand, the mode distribution is rather uniform and homogeneous. The laser beam was concentrated on small flat test samples via a focussing mirror, to achieve a constant focal diameter of approximately 15.5 mm (Spot size $1.89 \pm 0.1 \text{ cm}^2$). The focussing copper mirror had a diameter of 140 mm and a focal length of 1000 mm. **Fig. 1** is a photograph of the setup with the pendulum in open environment.

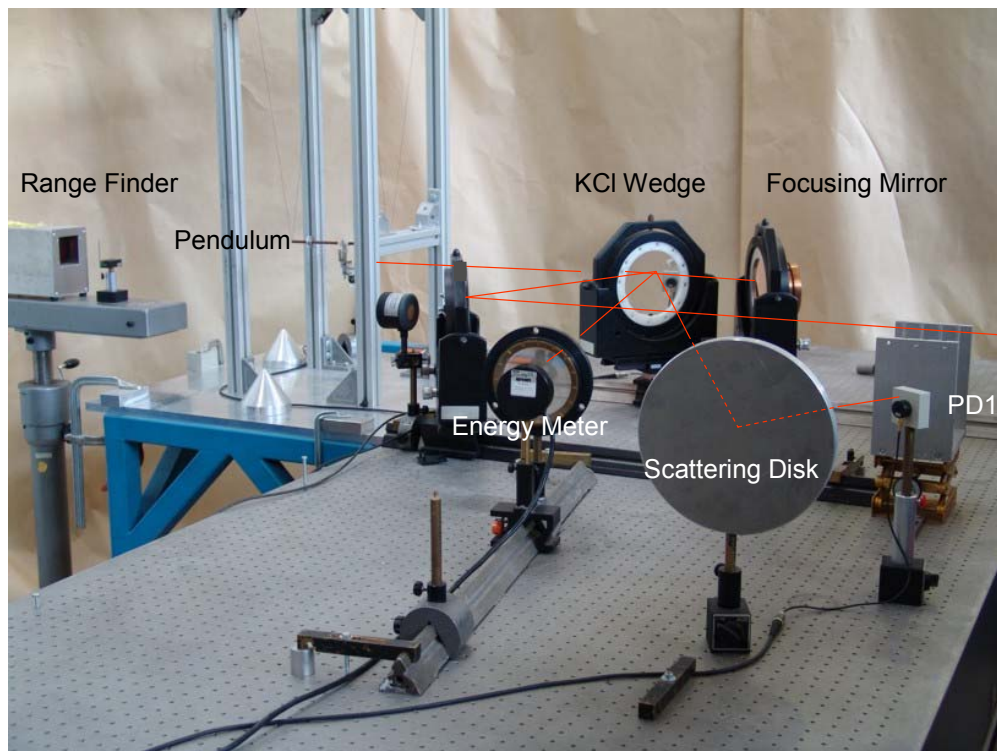


Fig. 1. Experimental Setup

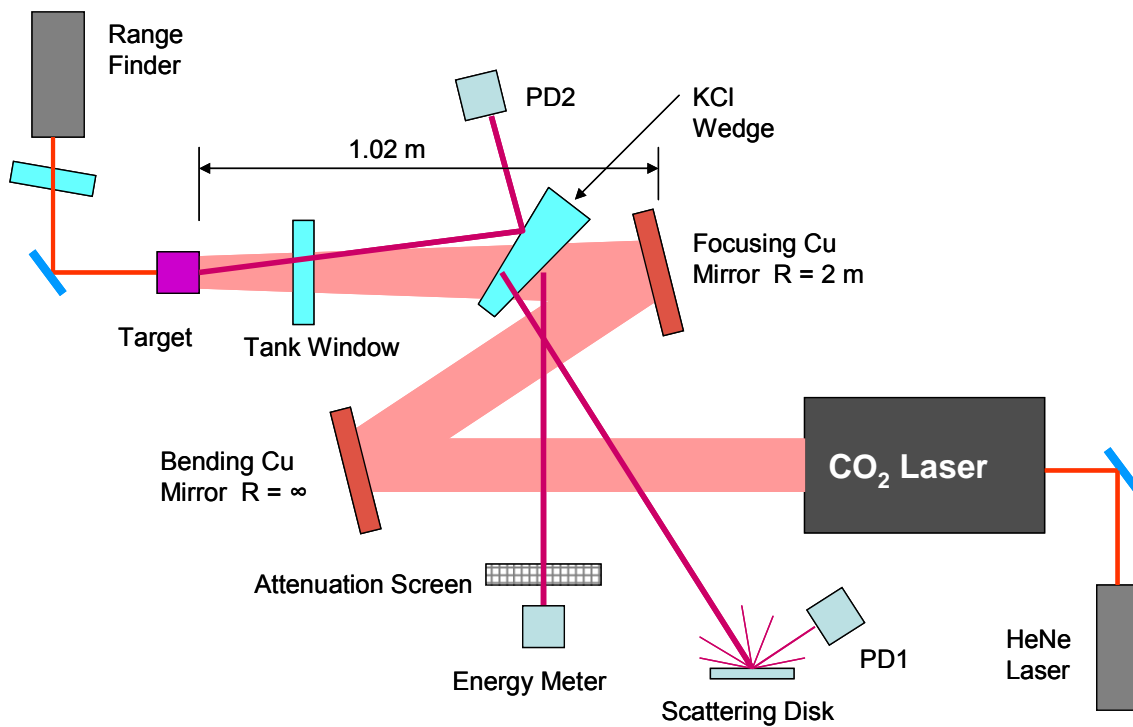


Fig. 2. Sketch of the optical arrangement

Fig. 2 shows the optical arrangement. The incident pulse energy from the laser is measured integrally as well as time resolved. The energy measurement was performed by an Ophir Laserstar with 2 channels and head PE50 BB, calibrated for $10.6 \mu\text{m}$. Before entering the energy meter, the signal intensity was reduced by a calibrated wire mesh. Time resolved measurements were performed with 2 Vigo photodetectors PEM-L-3 for $10.6 \mu\text{m}$ also. For this purpose, the laser beam was sent through a KCl wedge and the beam reflected from the surface on the sample side was sent to a sandblasted aluminum plate. The diffuse scattering was observed by photodetector PD1. The diffuse backscattering from the sample surface was reflected from the KCl surface on the sample side also and observed time resolved by the second photodetector, PD2. **Fig. 3** is another photograph of the mirror and photodetector arrangement, with the pendulum on the left side. The reading of the energy meter is directly fed into the data acquisition Pentium PC. The data acquisition and evaluation is carried out with Agilent VEE software.

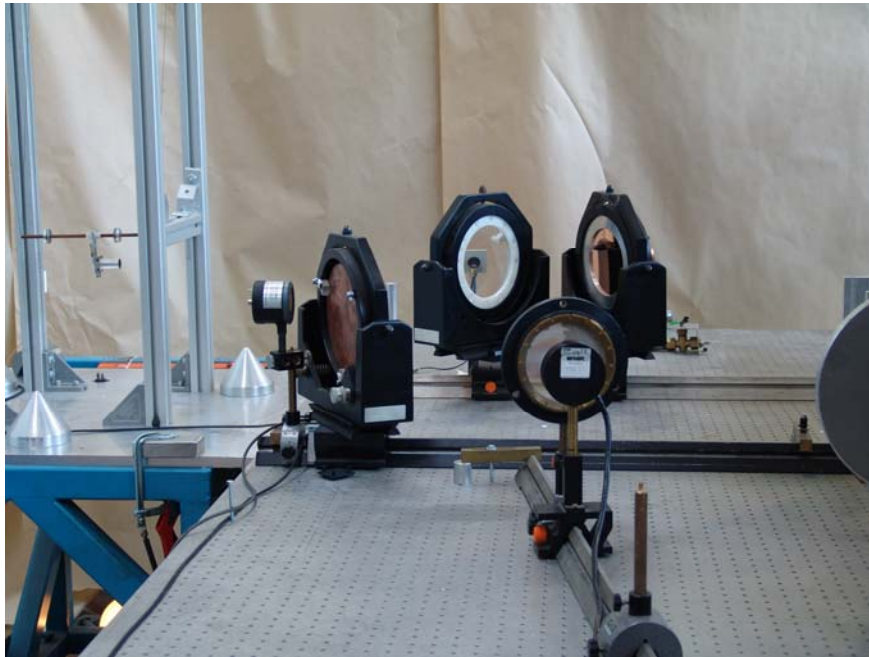


Fig. 3. Mirror arrangement

The time dependent measurement of the two power signals was intended for the demonstration of a continuous absorption of the laser pulse over the whole pulse length or likewise for the occurrence of a shielding effect due to laser absorption in the blown-off material. As discussed in chap. 4.5, the results from this measurement were not convincing. Since the curve looked too similar to the laser pulse curve, it was conjectured that some reflex of the laser pulse entered the detector more or less directly. However, this could not be proven. Another source could be the wedge itself, which may scatter some radiation. To prove that the measured reflex actually does not come from the target, the primary incident radiation of the laser pulse behind the KCl edge was sent far out of the range of any detector. Indeed, after a pulse energy of more than 120 J the detector measured a similar signal as the laser pulse again, though at a much lower level (see chap. 4.5). Therefore, at a later stage a different set of measurements was performed by looking at the signal that was transmitted through a small hole (diameter 3 mm) in the fixed sample. The transmitted laser beam hit a ceramic surface under 45° . The scattered radiation was then measured with the fast detector. Optical observation in air shows that a jet of luminous gas exits the hole to the rear side of the

probe. The detector is equipped with a BaF₂ window to cut off any radiation below a wavelength of 2 μm and should not see the radiation of the jet.

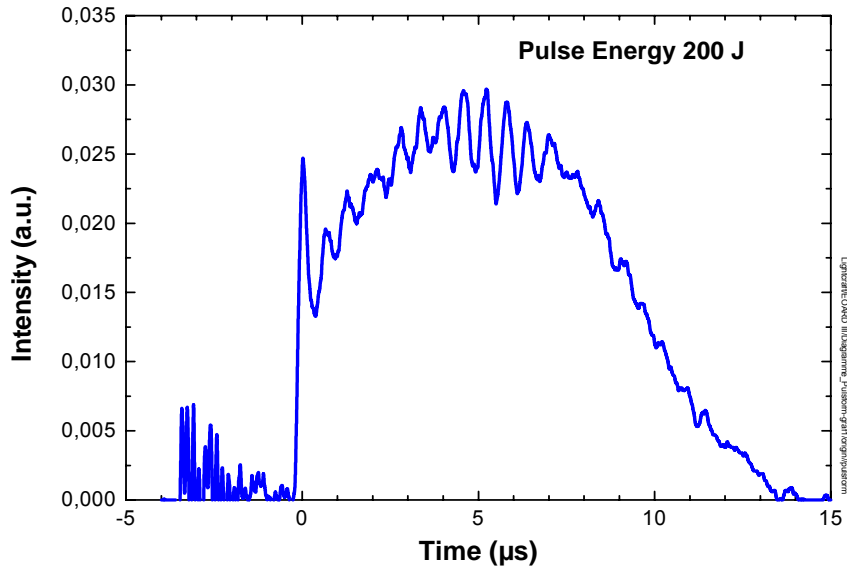


Fig. 4. Time dependent profile of the laser power

The laser pulse energy was varied between 40 and 280 J. The pulse length was close to 13 μs. The time dependent power profile is shown in **Fig. 4**. The laser pulse was shaped to mimic a double pulse as suggested in ref. 1, as good as possible. After a short spike, playing the role of the ablating pulse, the power rises again within 2.7 μs to a relatively flat maximum of 3.6 to 3.8 μs in length, before it decays to zero. After 13 μs the power is fallen to less than 5% of the maximum power. The remaining energy fraction is $\ll 1\%$ of the total energy. The integration over the curve for 200 J yields a maximum power of 20.3 MW and an incident intensity on the target of 10.7 MW/cm².

Hence, within the experimental range the numbers vary as follows

	Minimum	Maximum
Pulse energy	40 J	280 J
Fluence on target	22 J/cm ²	150 J/cm ²
Intensity on target	2.1 MW/cm ²	15 MW/cm ²

With respect to fluence, the parameter range begins where the numbers in ref. 1 end.

The samples were suspended on a pendulum to measure the mechanical impulse from the displacement of the pendulum as the reaction on the off-blowing material. The pendulum had a mass of 112 g and a length of 610 mm.

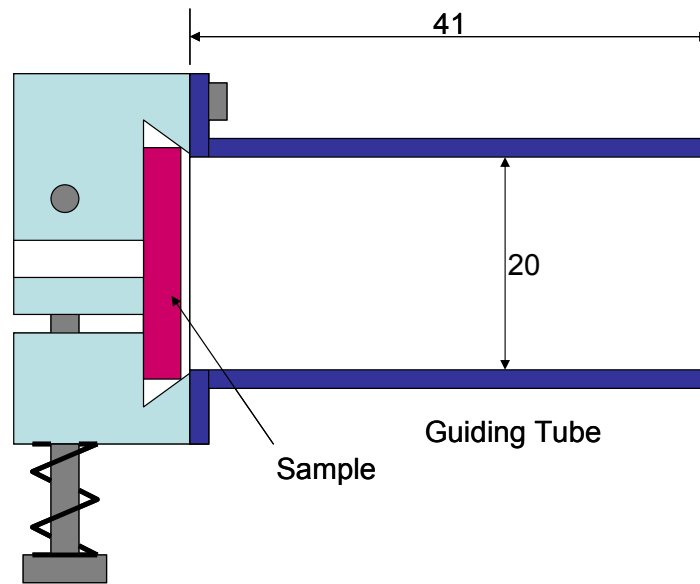


Fig. 5. Sketch of the sample holder with guiding tube

The sample holder has been newly manufactured for simple replacement of the flat samples and is fixed to the pendulum. It consists of two pieces connected by a spring and screw to hold the target sample, as shown in **Fig. 5**. Since the blow-off from a flat sample occurs in the 3-dimensional half-space, a one-dimensional expansion is enforced by placing a cylindrical gas guiding tube in front of the samples. **Fig. 6** is a photograph of the arrangement of sample and guiding tube. With 20 mm, the inner diameter of the tube was larger than the spot diameter (15.5 mm). This ensured that the incident laser beam did not touch the inner cylinder wall and produced no uncontrolled intensity distribution on the target surface. The arrival of the full pulse energy has been confirmed by 1. measuring the energy at the location of the target with and without the guiding tube; and 2. by placing thermal sensitive paper around the

sample. The result was in arbitrary units: without guiding tube 3.873 and with guiding tube 3.824, being well within the accuracy of the measurement. Only for a crude misalignment a shade was found outside of the guiding tube on the thermopaper. On the other hand, very close to the target surface, a 3-dimensional (3-D) expansion at the edge of the irradiated spot had to be accepted. However, with a length of 41 mm, the gas leaves the tube with a fully one-dimensional (1-D) direction, before it expands into the environment. It is believed that the 1-D setup produces maximum impulses, while the full 3-D expansion without the tube produces minimum impulses.

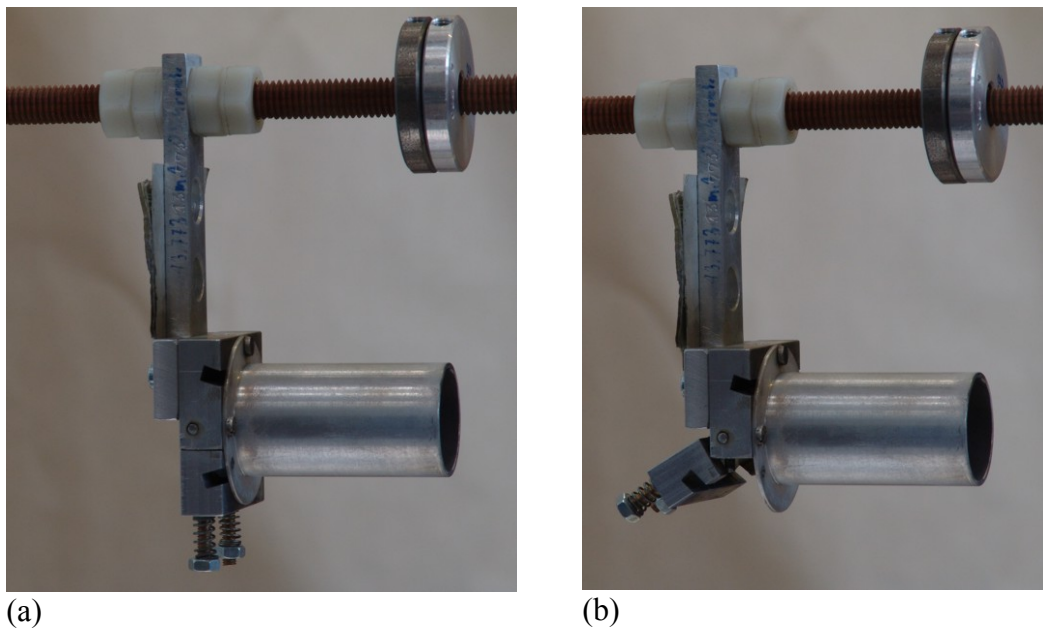


Fig. 6. Photograph of the sample holder in closed (a) and open position (b)

In general, the setup is similar to previous experimental investigations, as described in the according contract reports. The entrance window for the laser pulse into the vacuum tank has been modified by moving it further away from the target. This should help to reduce the deposition of blown-off material on the inside of the window. The KCl window was re-ground and had a diameter of 140 mm.

3. FORMULATION, ACQUISITION AND PREPARATION OF TARGET SAMPLES

3.1 Sample types

The acquisition and fabrication of the samples was difficult, since at first no manufacturer was willing to produce such specimens for us according to our specifications. Six companies had been asked. Finally, two sources could be found. The first source (BASF) provided us with samples of POM (polyoxymethylene=polyacetal) containing powder of either titanium or iron. This is a commercial product and is not modified to our desires. POM is at least the major constituent in "Delrin", which is a general brandname of Dupont. It is believed, that the difference to "Delrin" is negligible. Finally, a second source (Institute for Polymer Technology, Wismar, Germany) could be found to cast samples for us of POM with various contents of aluminum powder ($\leq 60\%$ by weight). In addition, butadiene with aluminum powder could be obtained from our rocket people and also Epoxy resin, in which we mixed ourselves aluminum and magnesium powder at various concentrations. The resin with proper hardener is a product for the shaping of aircraft skin structures in combination with various fabrics. The exact composition is company confident. The highest concentrations that we could produce were 40% by weight of magnesium and 50% by wt. of aluminum. Even higher concentrations become too tough for stirring and it is not possible to properly mix the two constituents. Also air bubbles cannot be removed anymore. The grain size of the Al and the Mg powder was less than 40 μm and, as can be seen in the micrographs, covers a whole spectrum. It is classified as "-325 mesh". Smaller sizes had been offered initially, but then could not be supplied upon our request for not exactly known reasons. For every polymer matrix, samples without powder content have been retained for comparison. – At a later state of the experiments and after evaluating the first results, additional resin samples with much lower contents of Al and Mg (3%, 5% and 10%) have been prepared.

Appendix 1 is a list of all samples and their characteristics. The samples with Fe and Ti have been delivered in a ring shape. The central hole was kept in the center, when producing the

actual sample shapes. The specific weights given in the table are only approximate values. Individual samples may deviate in their weight due to enclosed air bubbles.

Note: If not explicitly expressed, all compositions will be given in percent by weight. In order to find the composition by volume the appropriate ratio of the densities has to be applied. The measured density for POM is 1.40 g / cm^3 .

Samples with a size of $22 \times 22 \times 3 \text{ mm}^3$ have been machined from all specimens (**Fig. 7**). After cutting in size, the two large surfaces were equalized and ground by sandblasting to yield a smooth and plane surface. Some of the self-made samples showed a few small holes (typical diameter $\leq 1 \text{ mm}$), from air bubbles that were enclosed in the stirring and molding process.

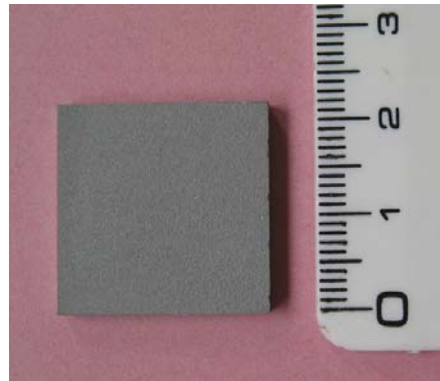


Fig. 7. Target sample

The samples were weighed with precision scales (Mettler AE 240) to within $\pm 0.4 \text{ mg}$. The typical weight of the samples ranges from 2 – 5 g depending on the metal content.

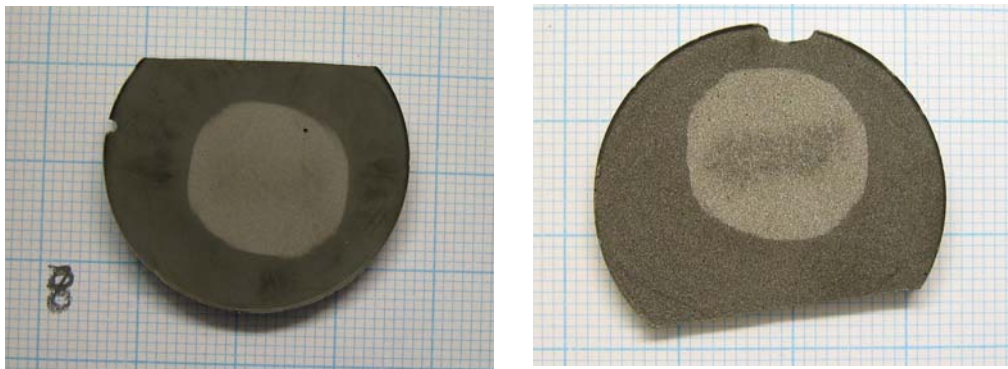


Fig. 8. Effect of several laser shots on Epoxy samples with 50% Al (left) and 40% Mg (right)

We have been warned by one manufacturer not to expose the specimens to laser radiation, because they may ignite and burn up furiously or even explode. Therefore, before the start of serial tests, small sample fractions of each specimen were irradiated by a laser pulse in steps of 1/8, 1/4, 1/2, 1/1 of the regular size to make sure that there is no danger of ignition. All specimens performed well and passed the test. **Fig. 8** shows resin samples with Al and Mg after about 10 shots at full energy (280 J). A marked change in color can be seen.

It should be mentioned that we did not succeed to melt POM in a way that it could be mixed with metal powders. One possible method could have been to use an extruder. Institutions (except for our final producer) that we asked to do this for us, refused with the argument of excessive wear on the mechanical parts of the extruder. As a consequence and before we found our final producer, we had also looked into other possible polymers, such as PET, PEEK, PI, PMMA, PTFE, PC, PE, Polysiloxan and Epoxy. For all these materials some laser ablation characteristics can be found in the literature, including a few examples for metal/polymer composites (ref. 8 – 15).

The following properties of Epoxy (Epon 28, Araldit) are taken from the literature: In ref. 13 a Q-switched Nd:YAG laser with maximum average output power of 75 W at a maximum repetition rate of 25 kHz was focused with a minimum spot size of 0.25 mm in diameter on metal/Araldit with a 50/50 vol% blend ratio. The purpose of this investigation was to look at the possibility of ablative machining of such compounds with lasers. Beside a mixture of Ni and Cr and some smaller amounts of other metals, one sample contained only Al powder with a grain size < 40 μm. This sample gave the lowest laser machining depth of all samples. Without an Ar gas assist jet the ablated polymer burned in air and waste material re-deposited on the surface. The mechanism of reaction is explained as energy transfer from the laser beam into the metal powders through absorption, then from the metal into the polymer through heat conduction. Apparently, the Al powder melted under the action of the laser, which required a temperature above 660°C in the composite material. A difference in the ablation rate has been found with steel dopant. If the powder grains were round and smooth the ablation rate was

larger than for grains with very irregular shape, because these grains can hook up and prevent expulsion. Dross is formed in this case.

3.2 Sample analysis under the electron microscope

All specimens have been observed under an electron microscope with various enlargements before undergoing laser irradiation. This was done in order to see the structure of the embedded powder, the grain size, and the homogeneity of the distribution and to compare later the laser treated surface picture with that of untreated material. All pictures of untreated material are made in the reflecting mode to discriminate the two constituents of the samples from each other. Morphological structures are not visible in this mode.

The picture gallery of all samples is found in **Appendix 2**. Note the scale size given in the bottom line of each photograph. A certain orientation of the flakes can be noticed for Al on some of the pictures. It is not clear if this is an effect coming from the mixing process or a smearing effect from the cutting of the probe. Parallel streaks across some of the pictures are scratches from the cutting process. Al and Mg flakes in the resin samples are irregular in shape and have a size distribution with some flakes being larger than 20 μm and others as small as 3 μm . Samples with more than 30% of metal appear as a metal composite where the polymer serves only as a binder. The structure of the metal powder of Al and Mg in the resin samples is completely different from that of iron (Fe) and titanium (Ti) in POM. The grains of these two metals are almost perfect spheres with diameters in the range of $< 1 \mu\text{m}$ to about 2 μm for Fe and 4 μm to 30 μm for Ti. The commercially acquired POM samples with Al show a different grain structure again: The grains are round, but elongated with an approximate ratio of the small side to the long side of 1:2 to 1:3 and more. The length varies from 7 μm up to 60 μm for some grains. In all cases the particle distribution across the whole sample cross-section appears fairly homogeneous, both, when looking at one spot on the sample with a lower magnification or when comparing different locations on a sample with each other. This is an indication that a sedimentation during the cooling process did not occur.

4. EXPERIMENTAL RESULTS AND INTERPRETATION

4.1 Measurements in air

The commercial POM samples with 0%, 20%, 40%, 60% of Al powder serve as baseline samples against which all other samples or arrangements are to be compared. In particular, these arrangements are measurements with unguided expansion into the half space, and measurements at reduced pressure in a vacuum vessel. All the latter experiments have been carried out with a lower number of values for the parameter pulse energy.

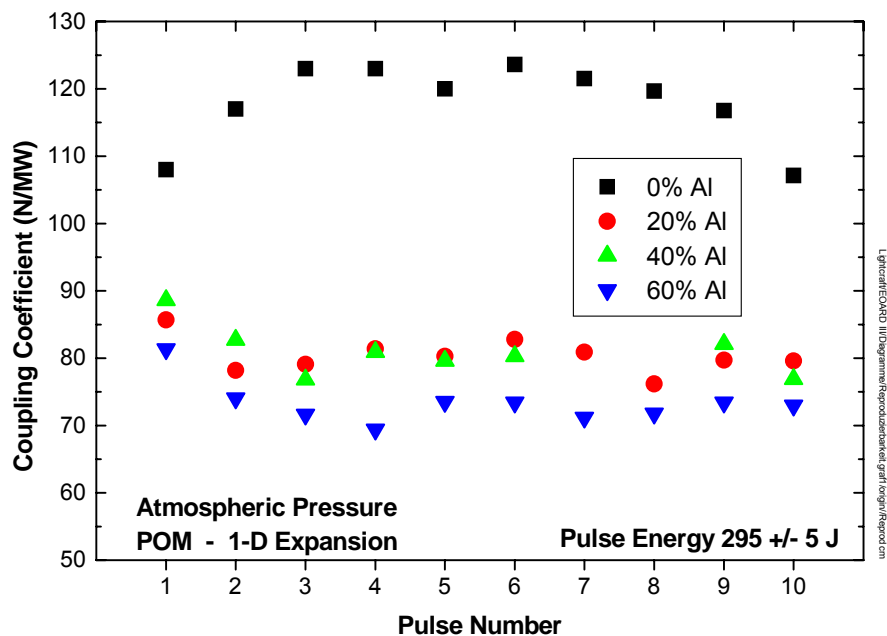


Diagram 1 Shot to shot reproducibility of the coupling coefficient

Reproducibility: The baseline samples were irradiated in 7 energy steps from 40 J to 280 J. The values of the energy are corrected for 6% energy loss at the KCl wedge. Each pulse was repeated 5 times with the same energy. For the impulse measurements with the pendulum the average of the last 3 laser pulses has been used as actual data point in the graphs. As **diagram 1** shows, the first two impulse values (here: coupling coefficient = measured

impulse / laser pulse energy) are generally different from all later pulses, indicating a conditioning effect. Therefore they were discarded. There is a fundamental difference whether the sample is plain POM or POM doped with metal. For POM with no metal the increase in measured impulse is 15% to 25% within 3 pulses; a decrease in impulse up to 8% is observed for all samples with Al.

Each sample was weighed before and after the 5 pulses. The weight loss per pulse was taken as the total mass loss divided by the number of pulses. The expansion was forced to 1-D by placing the probe inside the guiding tube.

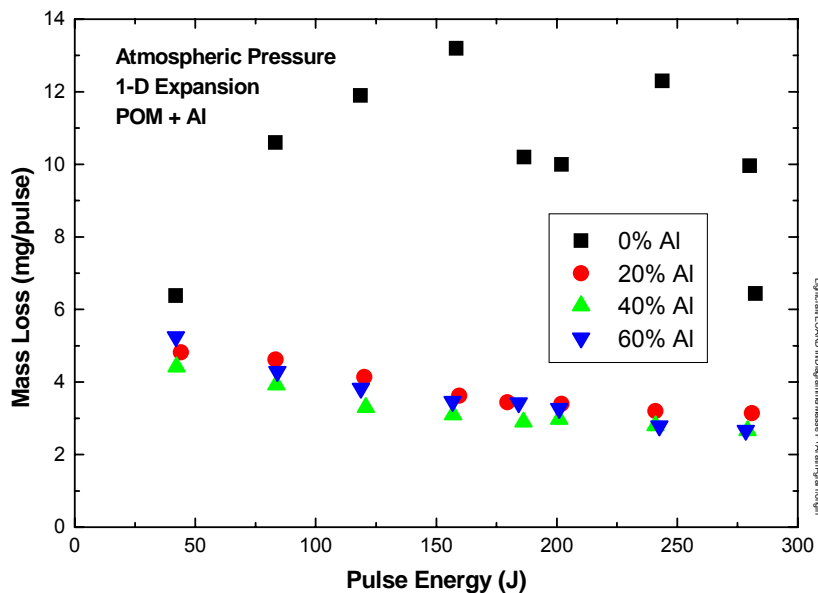


Diagram 2 Ablated mass vs. pulse energy

Ablated mass and deposited energy: The ablated mass as a function of laser pulse energy is shown in **diagram 2**. Samples with plain POM show an entirely different behavior as those with Al dopant. In fact, the amount of Al in the given range from 20% to 60% is almost irrelevant for the behavior of the ablated mass; the ablated masses differ by less than 20% over the whole energy range. It is surprising, however, that the ablated mass does not increase with the pulse energy, but rather drops. This is in contrast to the mass loss of plain POM,

which increases with energy to a certain level and then remains about constant (or decreases slightly), though with a large scatter. The ablated mass of plain POM is in the average about three times as high as for the doped POM. Since the point for 280 J seems to be too far out (lower value), a value from a later series (dependence of pressure) has been included in the diagram.

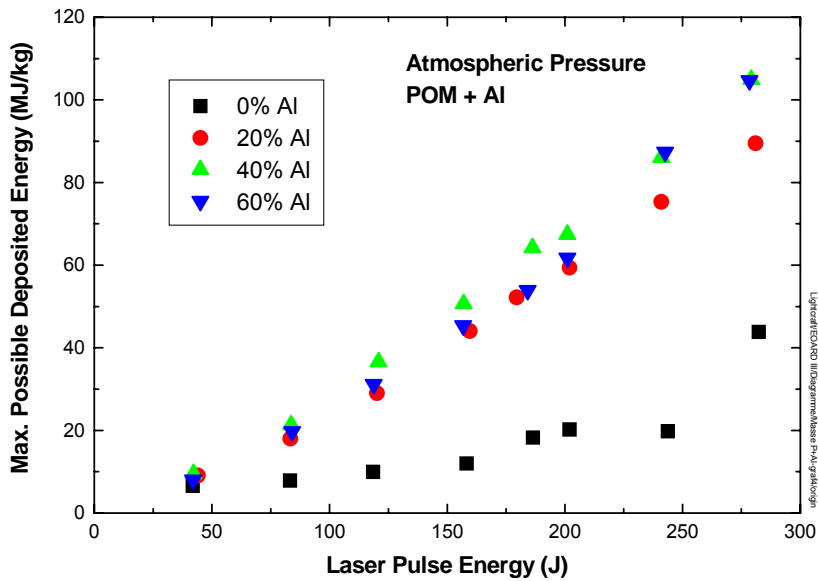


Diagram 3 Upper limit of deposited energy vs. pulse energy (air mass neglected)

If it is assumed - but need not be so for reasons to be discussed below - that all energy is deposited in the material, then the graph for the deposited energy (MJ/kg – pulse energy per kg of ablated mass) vs. laser pulse energy would look like shown in **diagram 3**. In this representation the deposited energy increases continuously with the energy and reaches values of more than 100 MJ/kg for the pulse energy of 280 J. However, it is not at all certain that the energy is dumped in the propellant only. If there is a breakdown in the air in front of the target, a significant amount of the energy may be deposited in an air plasma. If a detonation wave is developed, a large fraction of the energy may not reach the target surface after its development (see chap. 4.5).

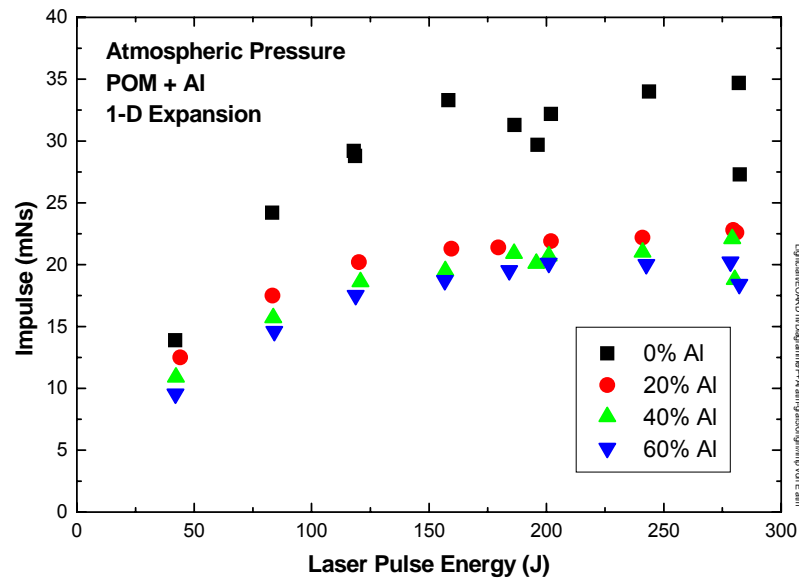


Diagram 4 Measured impulse vs. pulse energy

Impulse and coupling coefficient: Another directly measured quantity is the impulse (**diagram 4**). It increases with energy to about 150 J and then levels off. This is independent of the amount of metal dopant. However, as a consequence of the much larger amount of ablated mass, the impulse for plain POM is almost twice as high as that with Al dopant. Again the amount of metal does not influence the impulse significantly. Each data point is an average of 3 to 5 shots. The spread of the individually measured data is shown in **diagram 5** for plain POM and POM + 40% Al. Why the data scatter is larger for plain POM and certain pulse energy values is not known.

As a consequence of the trend of the impulse curve, the coupling coefficient shows the inverse behavior, as seen in **diagram 6**. The coupling coefficient decreases monotonically with increasing pulse energy. Samples of different metallic content show differences for low pulse energies and converge at the high energies. The maximum values are 230 to 300 N/MW for the doped samples and 340 N/MW for plain POM, and the minimum values are

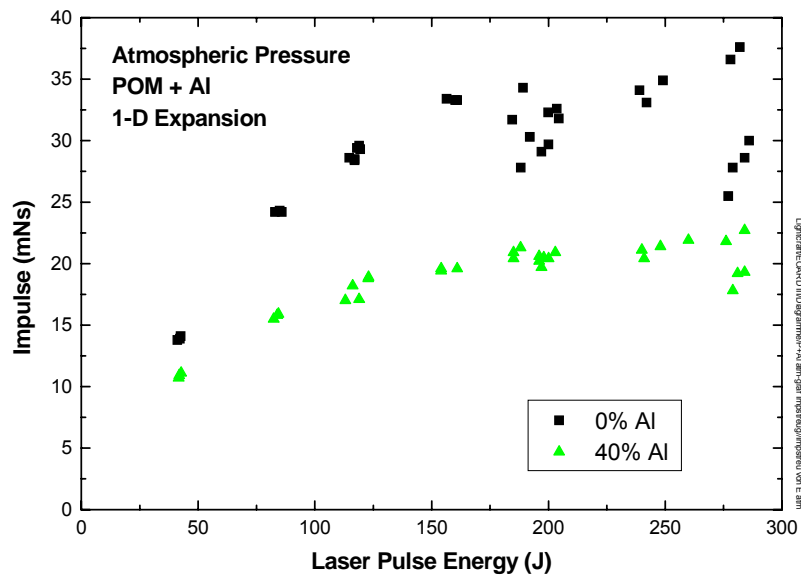


Diagram 5 Impulse data scatter of individual shots vs. pulse energy

75 N/MW for POM + Al and 140 N/MW for plain POM. All three diagrams contain a few data from another experimental series, but at otherwise equal conditions.

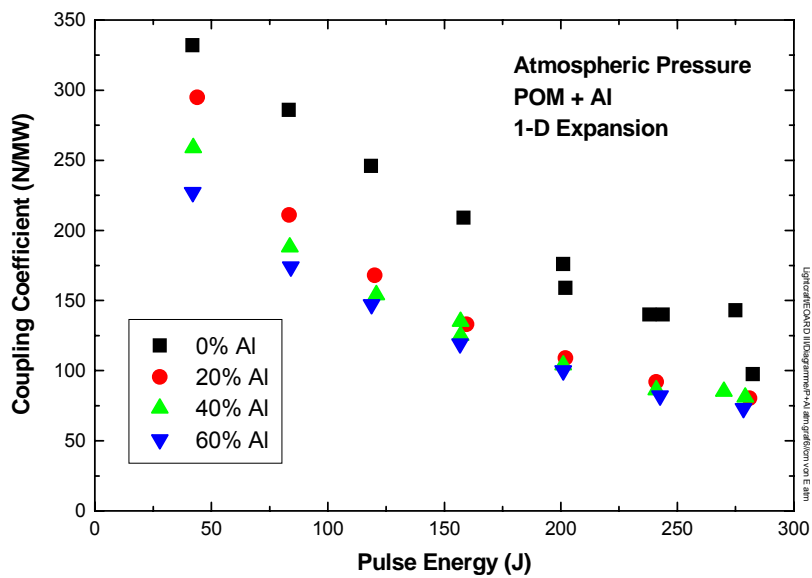


Diagram 6 Coupling Coefficient vs. pulse energy

Deduced quantities – Exhaust velocity: The derivation of the exhaust velocity, v_{ex} , is based on the balance of momentum: $v_{ex} = I / m_{ex}$, where I is the measured impulse that the pendulum has experienced and m_{ex} is the exhausted mass. The exhausted mass has to be distinguished from the ablated mass, since in the atmospheric environment surrounding air is necessarily accelerated as well. Because the amount of air is a priori unknown, only limiting values can be given. The maximum exhaust velocity, v_{max} , would be achieved, when only the ablated mass is exhausted. This is only the case in vacuum. On the other hand, an absolute minimum can be deduced by taking into account the full mass of air inside the cylinder of the guiding tube: $v_{ex} = I / (m_{abl} + m_{air})$, where again I is the measured impulse of the pendulum, m_{abl} is the ablated mass and m_{air} the air mass. The air mass at standard conditions is 16.6 mg and thus considerably more than the ablated mass - up to a factor of 5.5 when compared to POM + Al at high energies. In reality, however, not all the tube air is actually exhausted because the expansion stops, when the ambient pressure level is reached. The results for the minimum and the maximum possible velocities are shown in **diagram 7**. Since all curves for POM + n% Al will differ little, only the curves for 0% and 40% Al are shown.

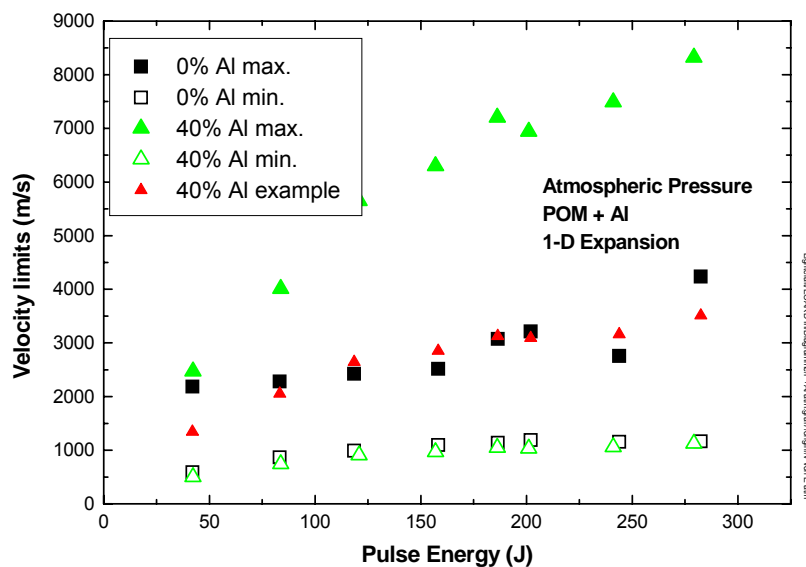


Diagram 7 Limiting values of the exhaust velocity vs. pulse energy in air. The values marked "example" are based on a reduced amount of exhausted air (see text).

The important specific impulse for propulsion applications is $I_{sp} = v_{ex} / g_0$ and thus roughly 1/10 of the velocity. While for the minimum velocity there is no difference whether the POM is doped with metal or not, the corresponding maximum velocity becomes twice as high with added metal powder. However, due to the large amount of air the difference between the maximum specific impulse of desired 800 s and as less as 120 s for the minimum I_{sp} is so significant that it does not allow safe extrapolations for application modelling. Even if, for example, in a real application only an amount of air, corresponding to a cylinder of height equal to the diameter of the ablation spot, is accelerated by the laser pulse, then the maximum specific impulse is calculated to 350 s (comparable to the max. spec. impulse of plain POM). The corresponding data in diagram 7 are marked "example".

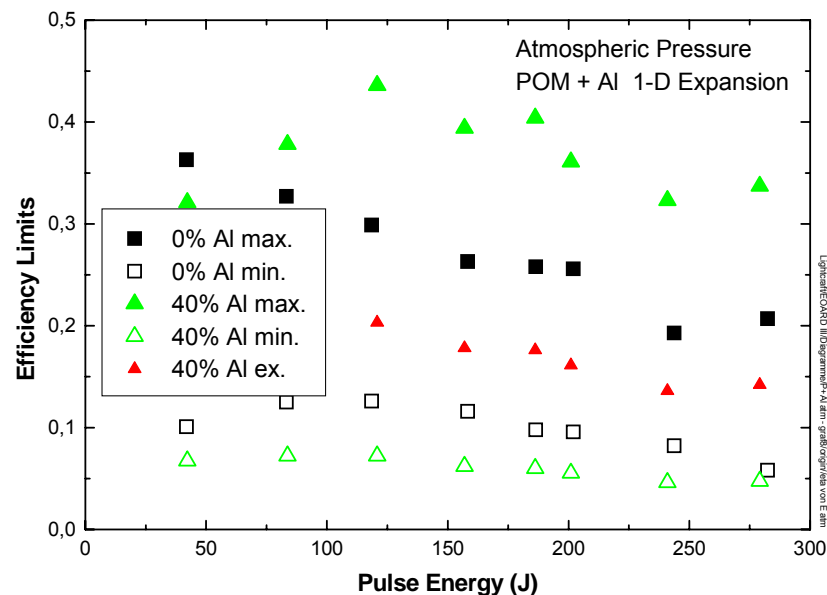


Diagram 8 Limiting values of the jet efficiency vs. pulse energy

Jet Efficiency: The jet efficiency is defined as $\eta = m_{ex} v_{ex}^2 / (2 E_L) = I^2 / (2 m_{ex} E_L)$. E_L is the incident laser pulse energy. The same discussion holds here as for the velocity. The result is shown in **diagram 8** in the same way as the exhaust velocity. The behavior of the curves will not be commented, except that there seems to be a weak maximum around 100 J. However, it

is noted that for plain POM the efficiency is bound between $6 \% \leq \eta \leq 36 \%$ and for POM + 40% Al between $5 \% \leq \eta \leq 44 \%$.

4.2 3-D effects

In the baseline measurements the gaseous exhaust has been forced to flow unidirectional by placing a guiding tube in front of the sample. This has been done for two reasons: If the diameter of the propellant surface of a flat plate thruster is large compared to the active flow distance of the gas then the flow is basically one-dimensional. In this case, the effective impulse and velocity will be maximum. The minimum situation is given for a 3-dimensional flow into the half-space in front of the propellant surface. The loss in performance has been measured for some selected parameters. In the following diagrams, the 3-D values for the mass loss and the impulse are entered into the previously displayed 1-D diagrams. The consequences for the quantities related to the laser pulse energy (deposited energy and coupling coefficient) are straight forward. Since exhaust velocity and jet efficiency are only extreme values they will also not be commented here.

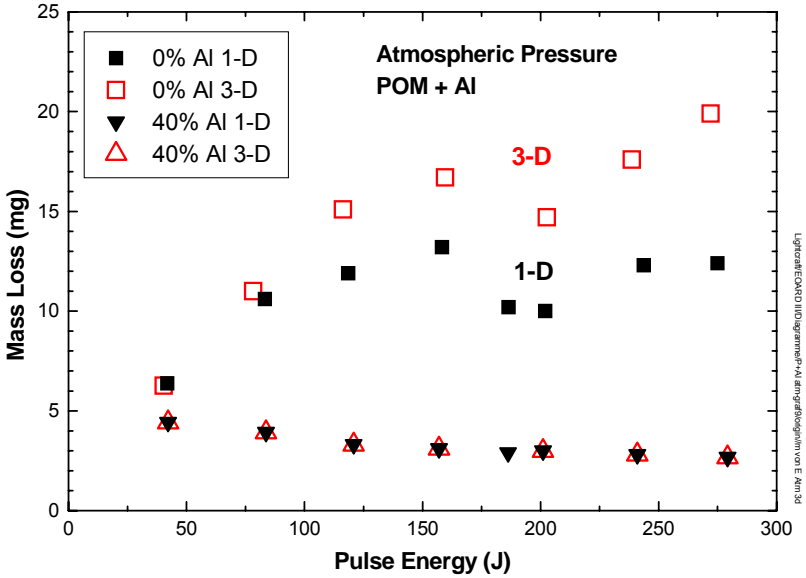


Diagram 9 Mass loss comparison

Mass Loss: The mass loss is plotted in **diagram 9** for plain POM and POM + 40 % Al for the one-dimensional and the three-dimensional case. While there is no difference for the doped POM, the mass loss for plain POM is higher in the 3-D case. This can only be understood, if some absorbing material expands sideways and with that gives room for more laser radiation to irradiate the surface. Perhaps noteworthy is the dip in the curve for plain POM at an energy of 200 J. It appears coinciding in the 1-D and the 3-D situation. This gives it some probability that it is not just a straying of data but may have some physical meaning, although it is difficult to understand.

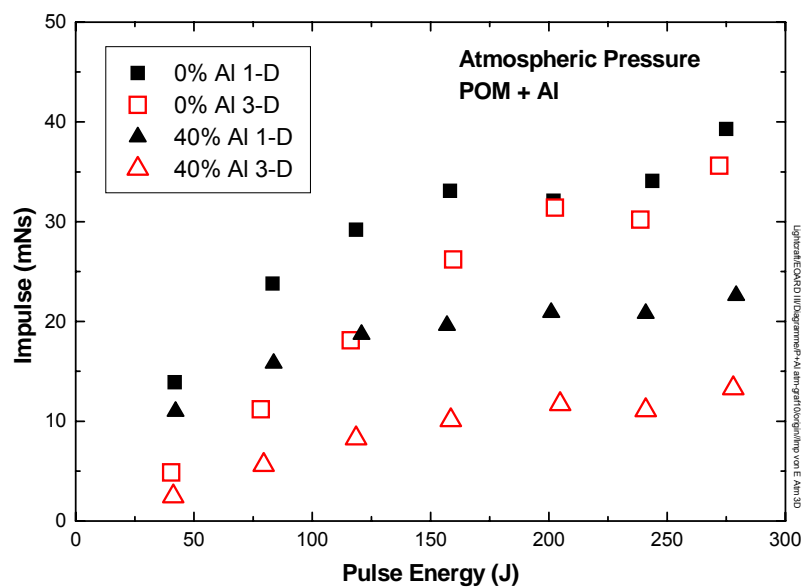


Diagram 10 Impulse comparison

Impulse: The impulse is shown in **diagram 10** for the the same parameters as for diagram 9. It is not surprising that the impulse values in the 3-D case are lower than in the 1-D case, because the impulse relevant velocity vector perpendicular to the target surface is necessarily smaller in the 3-D expansion. Thus, we have confined the range the velocity can vary for a certain pulse power, irrespective of the expansion dimension.

It is observed that the difference in impulse between the two cases is about constant for the doped POM for all energies, but it decreases for plain POM as the energy becomes higher. The different behavior may be explained by a different importance of the quantities m_{ex} and v_{ex} that define the impulse. In the case of the metal rich composite the velocity is apparently the dominant factor. It is higher in 1-D case and it increases with energy. On the other hand, the mass loss is approximately equal and decreases slightly with energy. Hence, the difference in impulse does not change much as the energy is increased. In the case with plain POM the amount of ablated mass is more than 3 times as high and even increases with the energy. Therefore, it is the exhausted mass that dominates the magnitude of the velocity for plain POM.

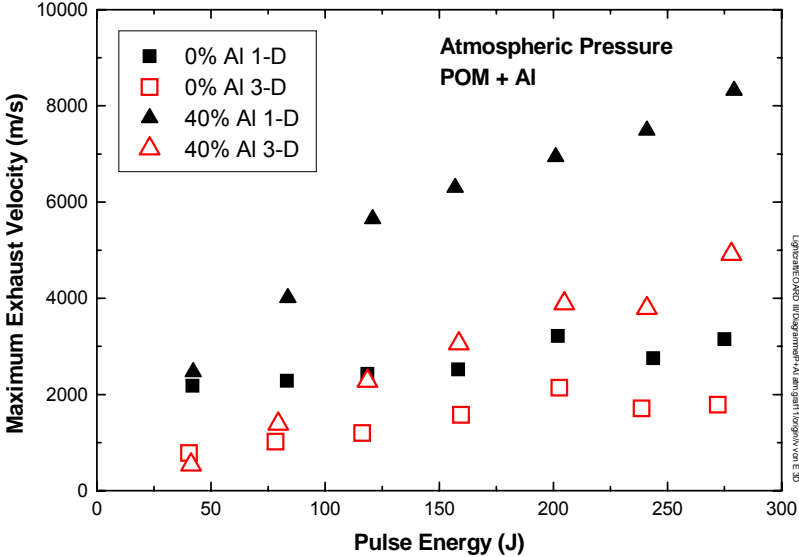


Diagram 11 Exhaust velocity comparison

Exhaust Velocity: Only the exhaust velocity based on the ablated mass is shown in **diagram 11**. In this extreme case the 3-dimensional expansion would reduce the exhaust velocity by a factor of 2 for both samples.

4.3 Measurements at reduced ambient pressure and in vacuum

Mass Loss: The measurements have been carried out in the vacuum tank for POM (+ Al) at various pressure levels. With 280 J, the pulse energy was the same in all experiments and the expansion was one-dimensional. A problem arose with the plain POM at pressures below 200 mbar. Most of these samples broke and it was difficult to weigh the remnants without loss of material. This led to incredible results for the mass with consequences for all derived parameters. The whole series has been repeated for the plain POM. Unfortunately, there is now a large discrepancy to the data of the first series. Both series have been included in the following diagrams. In the second series more values have been gained in the pressure range below 200 mbar. Yet, the scatter remains large. **Diagram 12** shows the dependence of the ablated mass per pulse as a function of the ambient pressure for samples with various Al concentrations.

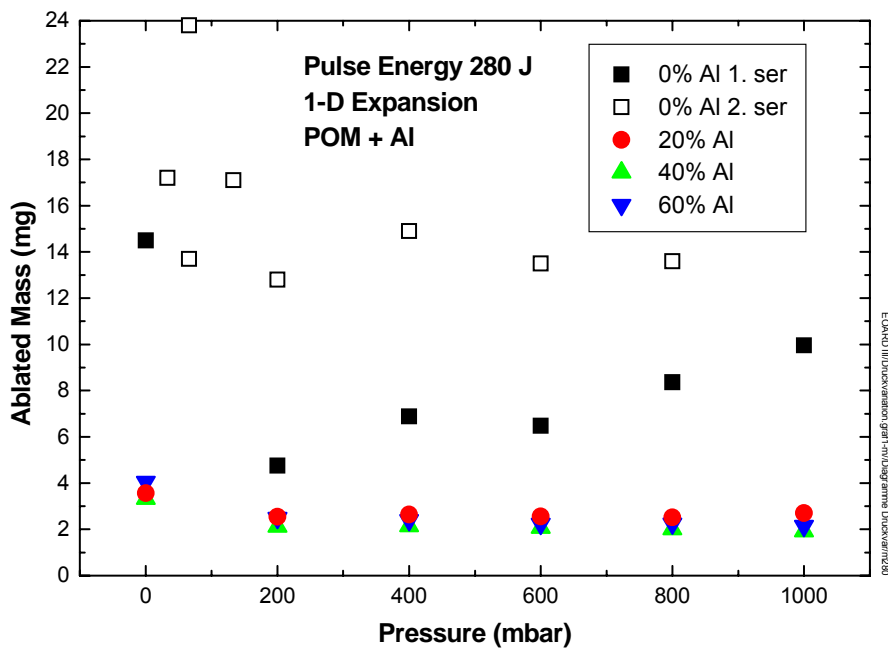


Diagramm 12 Ablated mass per pulse at a pulse energy of 280 J vs. pressure

Due to the large discrepancy of the two data sets for plain POM it is difficult to make out a trend. It is interesting to note that for Al samples with Al content the ablated mass is virtually

independent of the metal concentration and the pressure, except for pressure zero. Here a markedly higher ablation rate was found. If this tendency holds also for plain POM, as suggested by the second series, then the ablation rate is many times higher if metal is added, as has been found already at atmospheric pressure. **Diagram 13** is a close-up of diagram 12 and shows only the data for POM + Al in more detail.

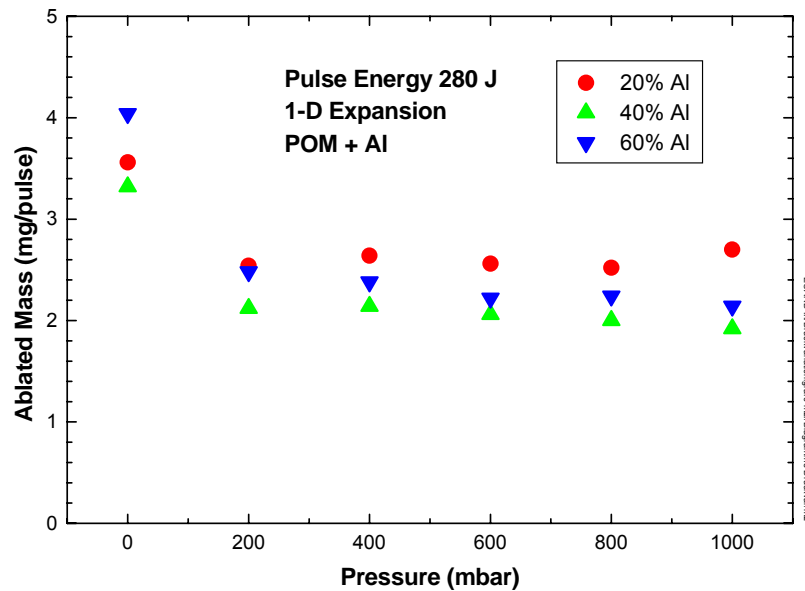


Diagram 13 Ablated mass for Al doped POM vs. pressure

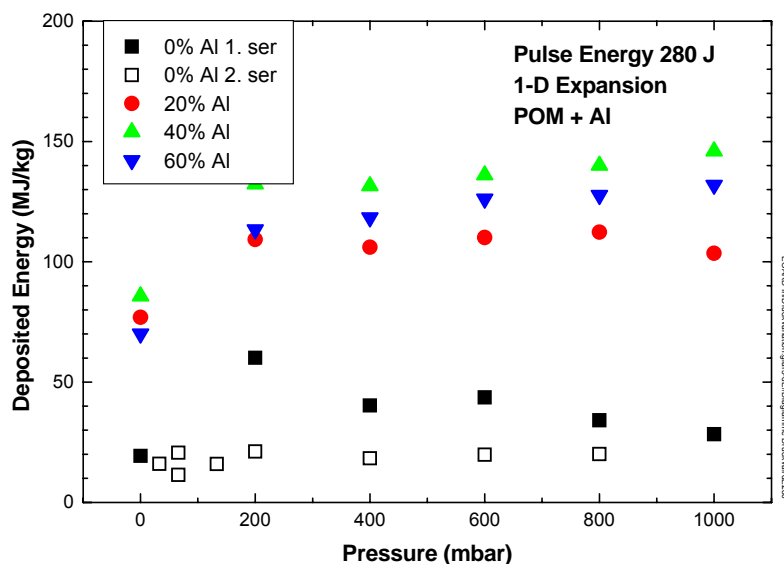


Diagram 14 Apparent deposited energy vs. pressure

Derived from the ablated masses the apparent deposited energy is shown in **diagram 14**. These numbers are gained on the assumption that all incident laser energy is actually deposited in the solid material. This, however, is not the case.

Coupling coefficient: Since the pulse energy is constant, only the coupling coefficient is shown in **diagram 15**.

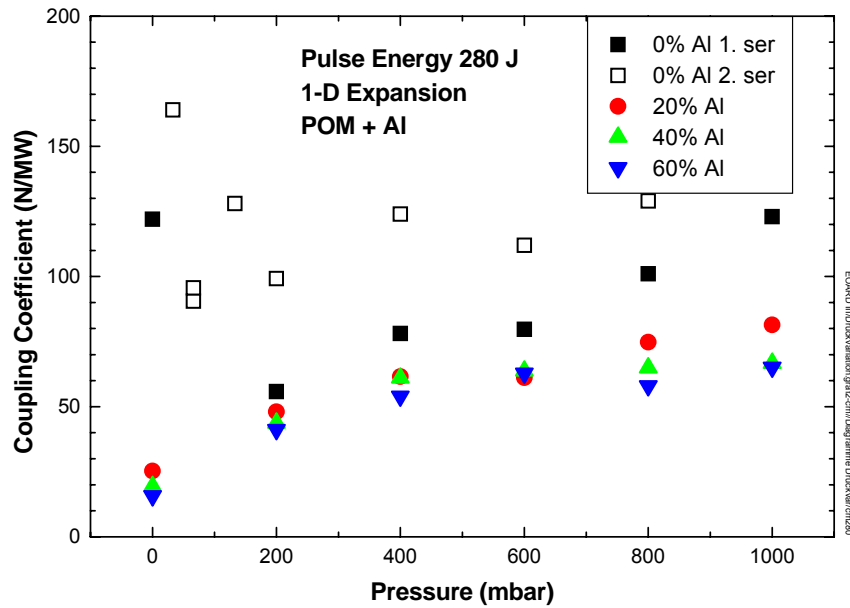


Diagram 15 Coupling Coefficient vs. pressure

The values for the coupling coefficient are remarkably low and below 500 mbar they drop with the pressure. Again there is little difference between different metal concentrations. Obviously, the increased ablation at pressure zero, as seen in diagram 13, does not result in a higher impulse and coupling coefficient. On the other hand, the larger coupling coefficient for plain POM is a direct consequence of the higher ablation rate.

Velocity and Jet Efficiency: These two quantities depend on the complete accelerated mass, including residual air. Only for full vacuum the numbers are real. Exhaust velocities in vacuum for metal doped POM do not exceed 2000 m/s and are the higher the lower the Al

concentration is (diagram 16). Also the jet efficiency in vacuum becomes extremely low (diagram 17).

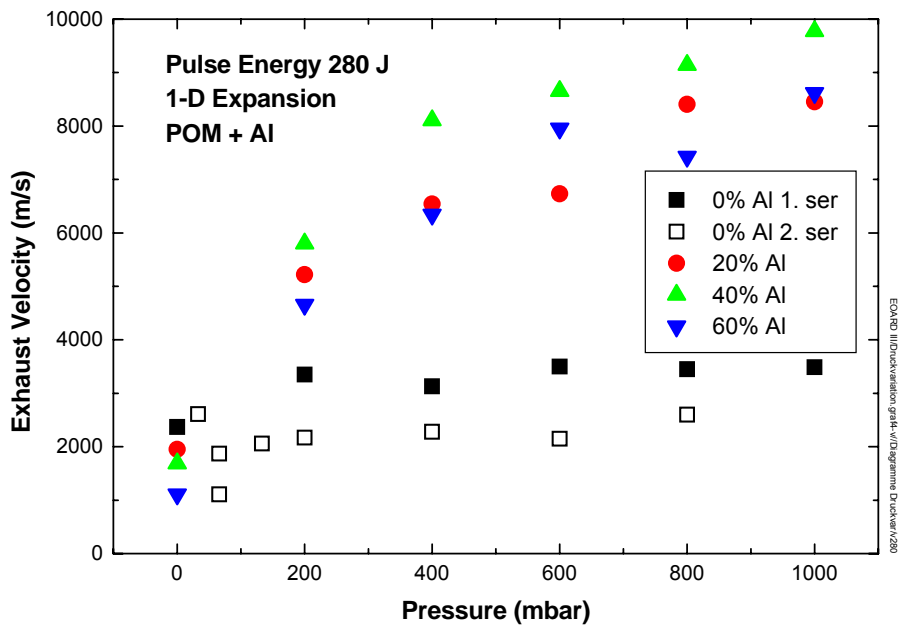


Diagram 16 Apparent exhaust velocity vs. pressure

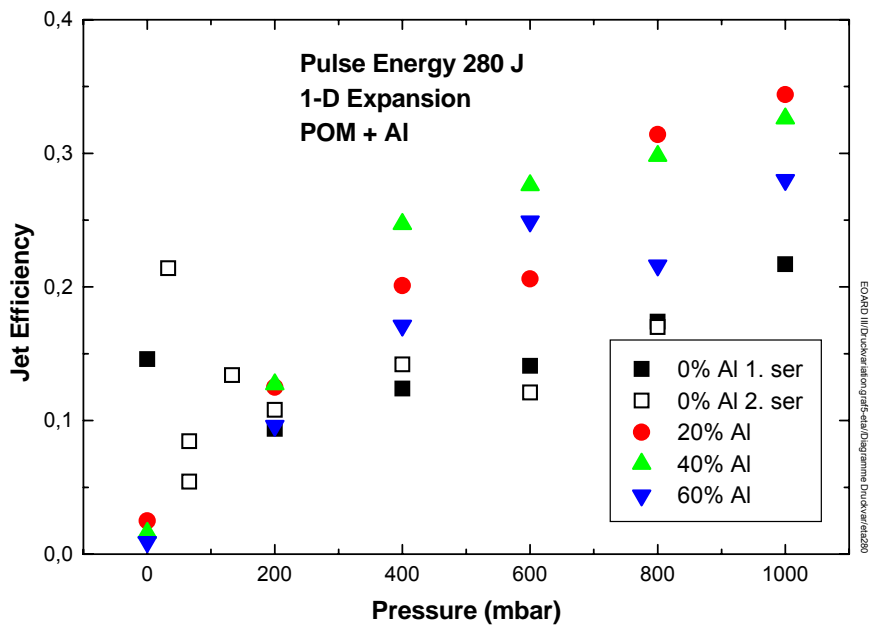


Diagram 17 Apparent jet efficiency vs. pressure

In the following diagrams the dependence on pulse energy is shown at 3 different pressures for plain POM (black symbols) and POM + 40% Al (red symbols). The latter is considered representative for all Al concentrations. The pressures were: $p = 1000$ mbar (atmospheric pressure); 400 mbar; and 0 mbar (vacuum). Only 3 energy values have been applied, in order to limit the amount of data (120 J, 200 J, and 280 J). Also included in the diagram for comparison are measurements without the guiding tube (open symbols, designated as 3-D expansion and slightly offset from the 200 J value). Again, of the derived quantities only the vacuum values are correct (square symbols).

Ablated Mass and Deposited Energy (Diagrams 18 and 19):

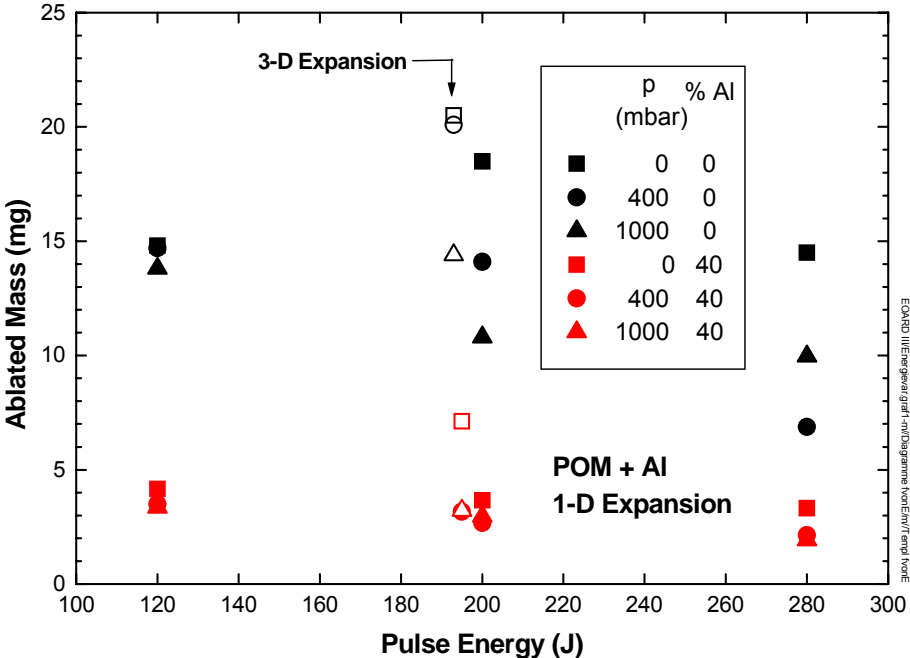


Diagram 18 Ablated mass per laser pulse under various conditions of pulse energy, ambient pressure and expansion geometry for POM with and without metal content

Note that the ablated mass is generally decreasing with increasing pulse energy. This is an indication of an energy dependent absorption mechanism outside of solid sample body.

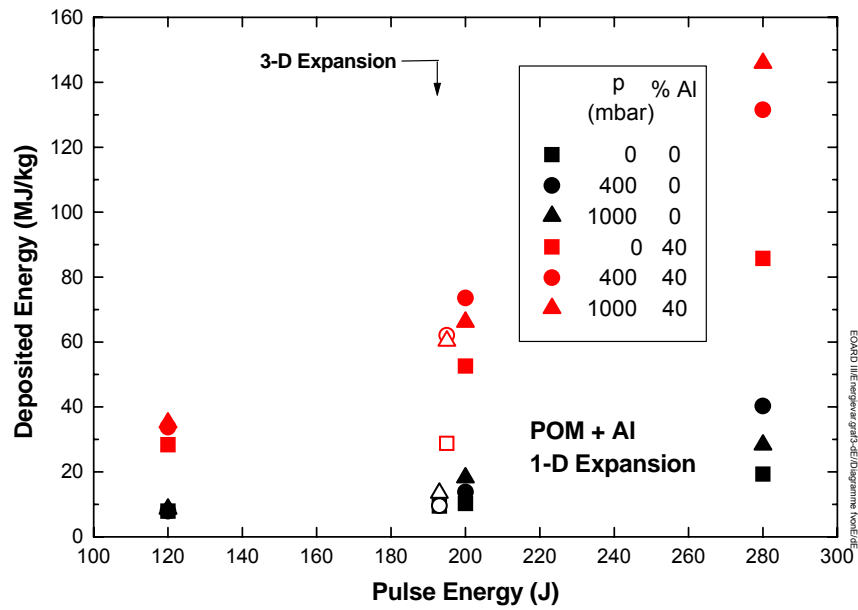


Diagram 19 Apparent deposited energy, as derived from the data of diagram 18, vs. pulse energy

Coupling coefficient (Diagram 20): As the ablated mass, the coupling coefficient is decreasing with the pulse energy.

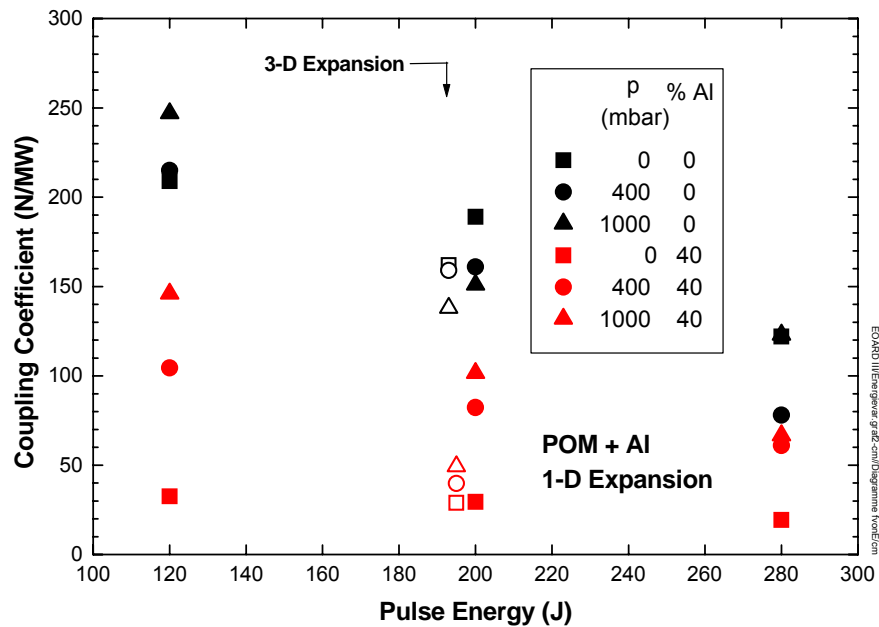


Diagram 20 Coupling coefficient vs. pulse energy

Jet Velocity and Efficiency (Diagrams 21 and 22): Only data for vacuum represent real values.

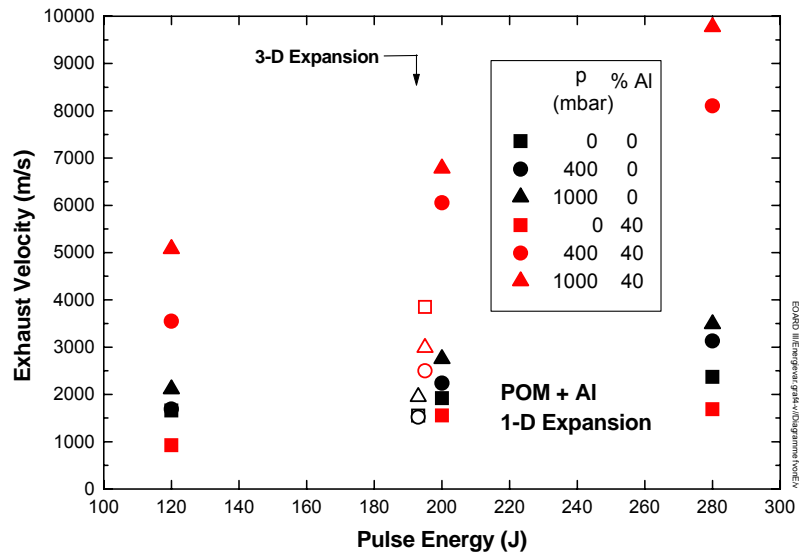


Diagram 21 Apparent jet velocity vs. pulse energy

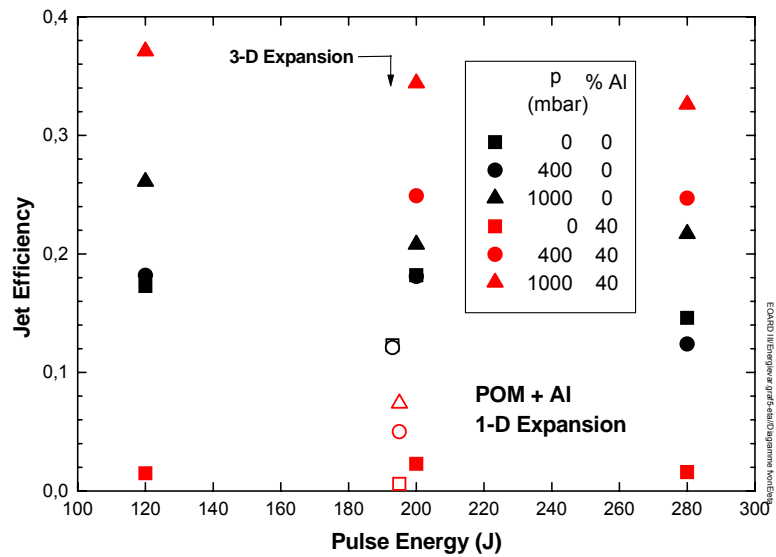


Diagram 22 Apparent jet efficiency vs. pulse energy

4.4 Comparison of different sample formulations

All samples have been compared under the same conditions at a pulse energy of 200 J. Shown are values for atmospheric and for vacuum environment. The pulse energy varies by +6 J / -4 J in atmosphere and 0 / - 7.6 J in vacuum.

The samples are numbered as follows:

Nos. 1 – 4	POM + Al
No. 5	Butadiene + Al (unknown amount)
No. 6	Epoxy + Al (unknown amount)
No. 7 – 14	Epoxy + Al
No. 15 – 20	Epoxy + Mg
No. 21	POM + Fe
No. 22	POM + Ti

If known, the concentration of metal is marked in the diagrams and increases from left to right in comparable composites. All measurements are made for the 1-D case. The samples nos. 21 and 22, with Fe and Ti content, are irregular due to a larger hole in the center. Therefore, all measurements of these two samples cannot be directly compared with the results of all other samples.

Mass and deposited energy: **Diagram 23** shows the mass loss per pulse. The mass loss for epoxy is very similar to POM when doped with aluminum at comparable concentrations. This is particularly striking in the difference between plain polymer and metal doped polymer. In order to bridge the large gap between composite and pure polymer it has been decided to produce new Epoxy samples with 3%, 5% and 10% of either Al or Mg, which are included in the diagrams as well. It is obvious that the mass loss decreases with increasing metal concentration. However, although in the new Epoxy samples the metal content was reduced considerably, there remains a large jump between the result for these low concentrations and for no metal at all. It is further observed that the mass loss decreases more pronounced in the Epoxy samples with increasing metal fraction than with the POM samples. Mg doped Epoxy samples show a strongly reduced mass loss, which is much more than the density ratio of the two metals Al (2.7 g / cm^3) and Mg (1.74 g / cm^3) would suggest. This is in particular so in

atmospheric environment. With respect to the higher density, the higher mass loss for the Fe (7.87 g / cm^3) and Ti (4.5 g / cm^3) doped is plausible. If Epoxy does ablate without noticeable residue, it would be an even more convenient propellant with respect to fabrication than POM.

Another result is the fact that in vacuum the ablation rate is drastically increased. This is particularly obvious for the resin samples.

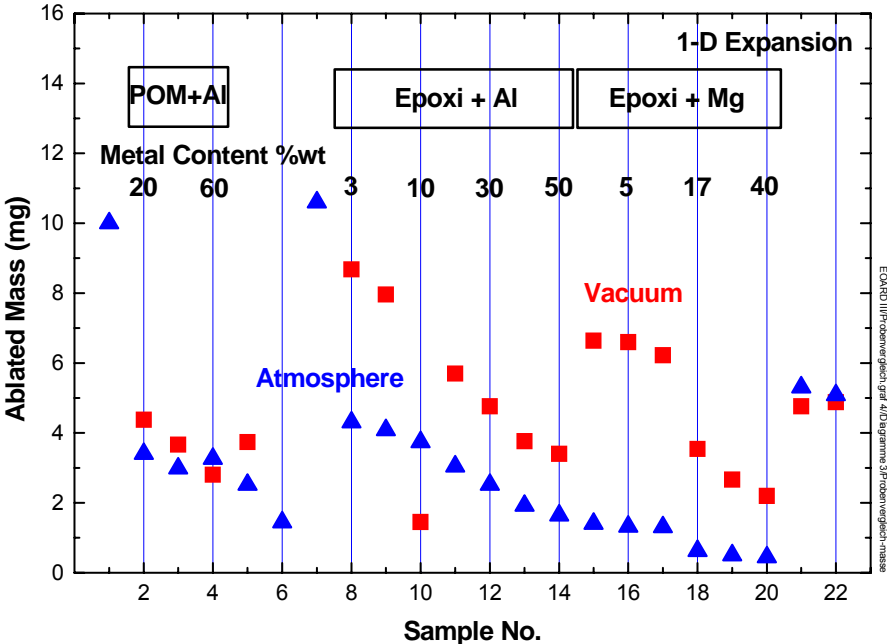


Diagram 23 Comparison of the ablated mass per pulse at a pulse energy of 200 J for different material samples. For the detailed specification for each number see the text and Appendix 1

The deposited energy in **diagram 24** is related to the laser pulse energy and may be different when taking into account the actual energy arriving at the target. Note, that the vertical axis is in logarithmic scale. At atmospheric pressure the deposited energy for doped material is 3.5 to 6 times as high as in the undoped material and another factor of 3 and more is found for the dopant magnesium compared to aluminum. In that respect, Mg would be a particularly

favorable metal dopant. The curves are the inverse of the ablated mass multiplied by the pulse energy and consequently the deposited energy in atmosphere appears to be higher.

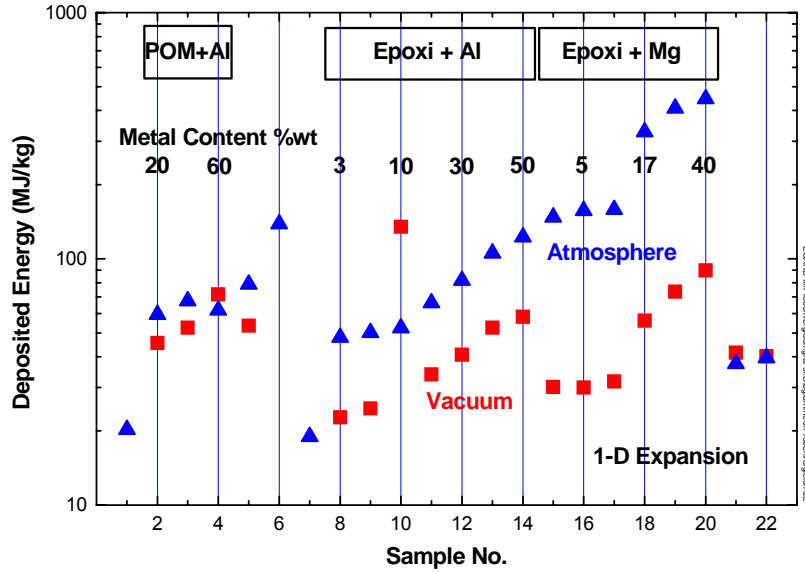


Diagram 24 Comparison of the deposited energy

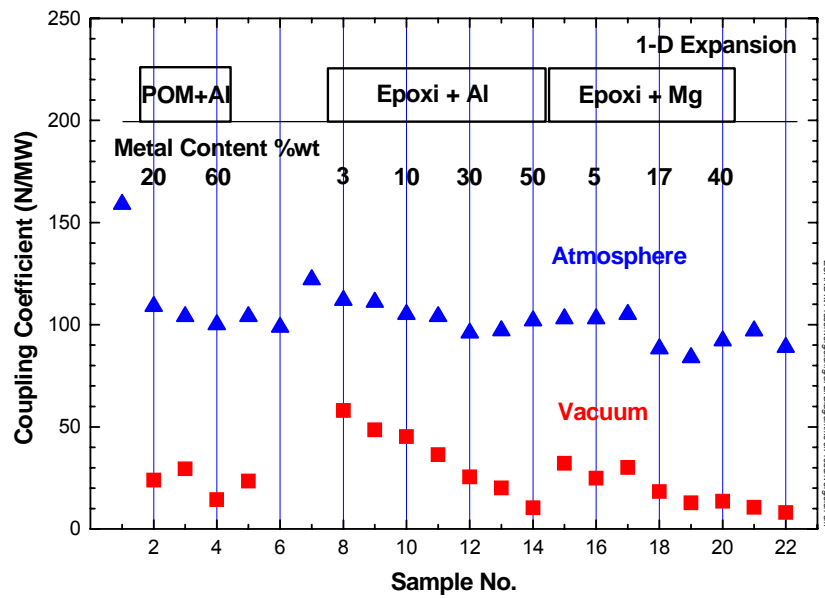


Diagram 25 Comparison of the coupling coefficients

Coupling Coefficient: The coupling coefficient is shown in **diagram 25**. It is remarkably equal for all the doped samples and within experimental error has a value of 100 ± 10 N/MW at atmospheric pressure. In vacuum it decreases with increasing concentration of metal and is generally less than 50 N/MW.

Jet Velocity and Efficiency: Following the earlier discussion the derived velocity in ambient air is only a limiting value and of no practical use. Therefore, only the velocity in ambient vacuum is presented here (**diagram 26**). A general trend is a decrease of the velocity with increasing metal content. However, the data scatter considerably and do not exceed the range from 800 m/s to 1500 m/s. This is far from the anticipated values of about 8000 m/s.

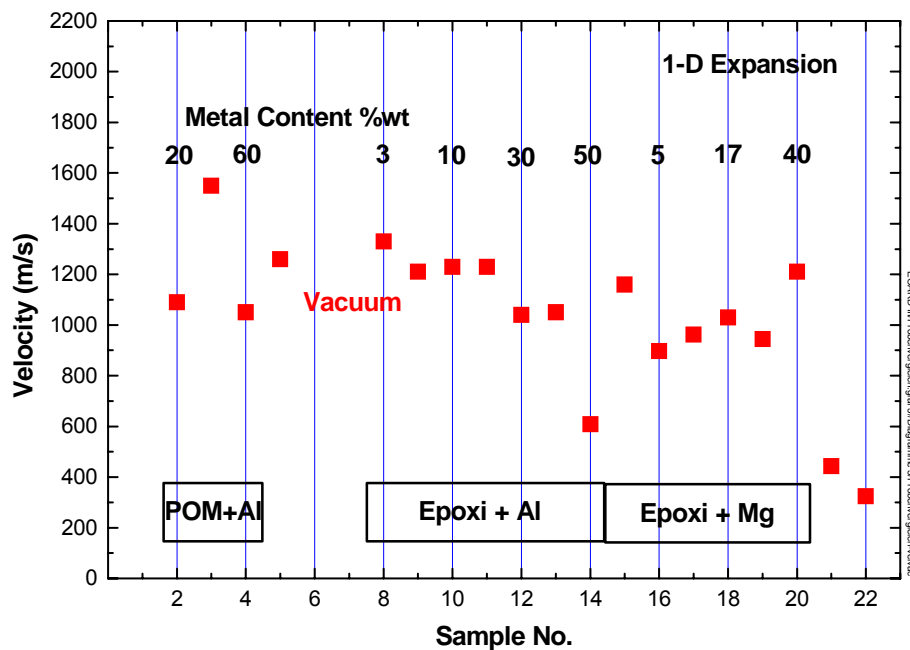


Diagram 26 Comparison of the jet velocity

Like the velocity, the jet efficiency is meaningless for ambient atmosphere. In fact, for Mg as the dopant the values would even be greater than one. The jet efficiency for the 1-D expansion

in vacuum is shown in **diagram 27** and is also found to be extremely low. As the velocity, it decreases with increasing metal content.

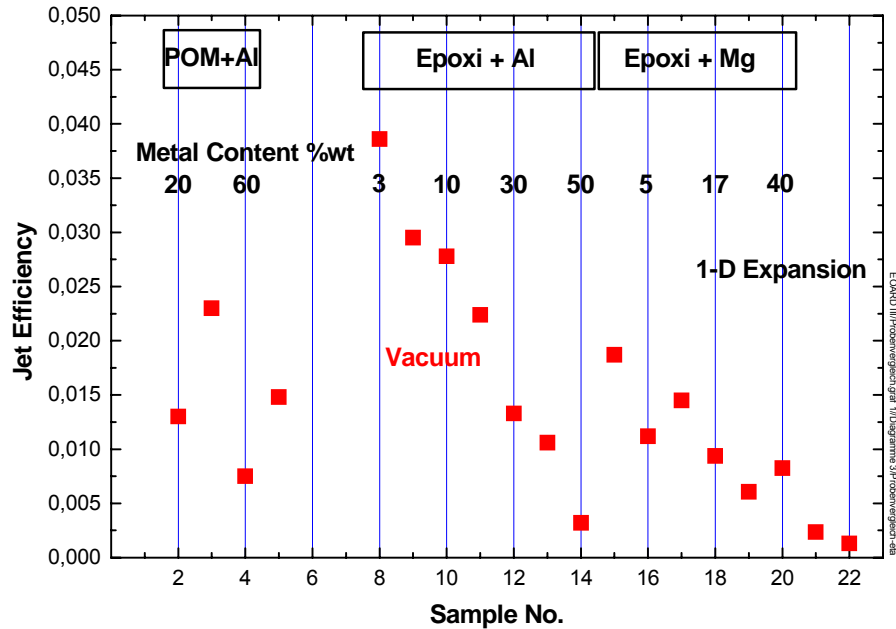


Diagram 27 Comparison of the jet efficiency

4.5 Time resolved power measurements

The following **diagrams 28 and 29** show time resolved signals from the incident laser pulse ($E(t)$ – black curve) and for the signal that was originally believed to be reflected from the sample surface during irradiation ($R(t)$ – red curve). The units are arbitrary and not equal for the two curves.

It has been checked by covering up the detector that the signal of the reflection is not an electric stray signal from the laser discharge. However, it still follows too closely the incident laser signal to be believable. Also the general trends of the various ablation parameters as a

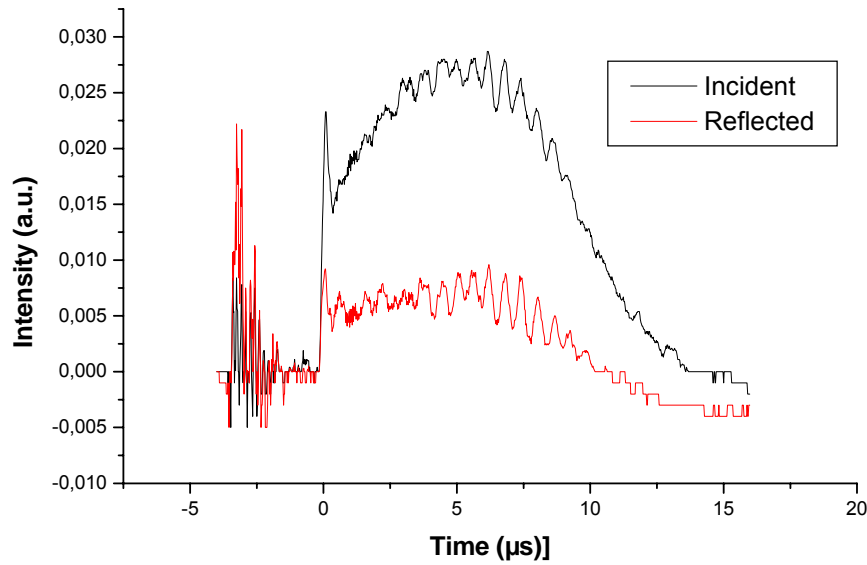


Diagram 28 Laser pulse on undoped POM with an energy of 200 J.

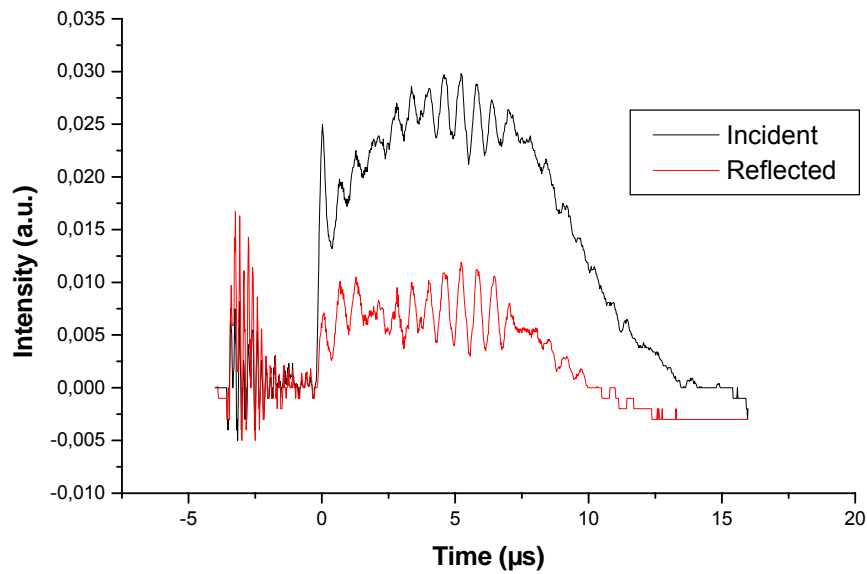


Diagram 29 Laser pulse on POM with 40% of Al at an energy of 200 J

function of pulse energy cannot be understood if not some absorption in a plasma wave, decoupled from the target, is going on. The incident beam was therefore sent through the KCl wedge into infinity without hitting the target. In this case, detector 2 for the reflected signal

saw also a signal when the pulse energy was higher than 100 J. The following two diagrams 30 a and b show the new signal for 2 different pulse energies without the presence of a sample.

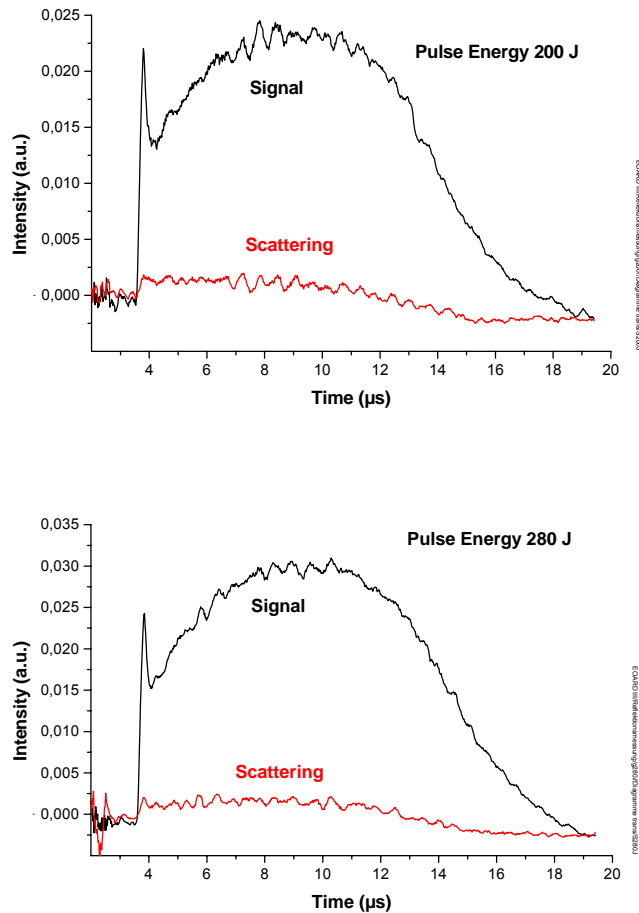
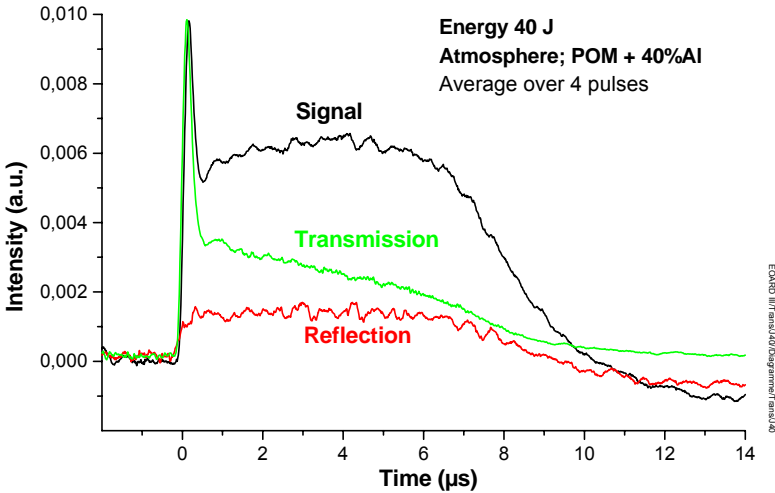


Diagram 30 Time resolved power signals for a pulse energy of 200 J (above) and 280 J (below) with target removed.

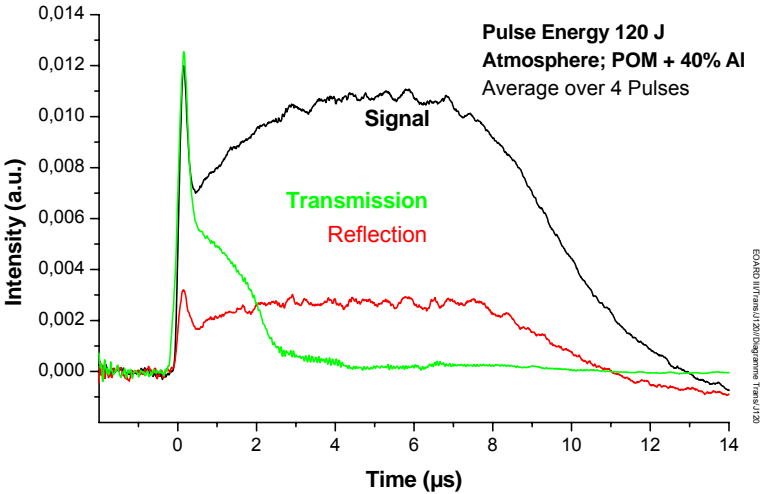
It can be seen from these 2 graphs, that the signal on detector 2, denominated “scattering”, is much lower than when a target is present. It is also seen that the scattering signal grows as the total energy grows. The conclusion is, that there is some scattering present indeed, probably coming from the wedge, but the reflection from the target seems to be considerably greater.

In order to resolve the question about the actually arriving power on the target as a function of time and the role of a possible development of an absorbing (and reflecting) plasma cloud in front of the target a hole of 3 mm in diameter was drilled in the center of a POM sample with 40% Al. The power transmitted through the hole was monitored by placing one of the detectors behind the sample. This detector should only see light that actually arrives on the surface of the sample. These experiments have been carried out in atmosphere at various energy levels. The result for different pulse energies is seen in the following **diagrams 31 a – d.**

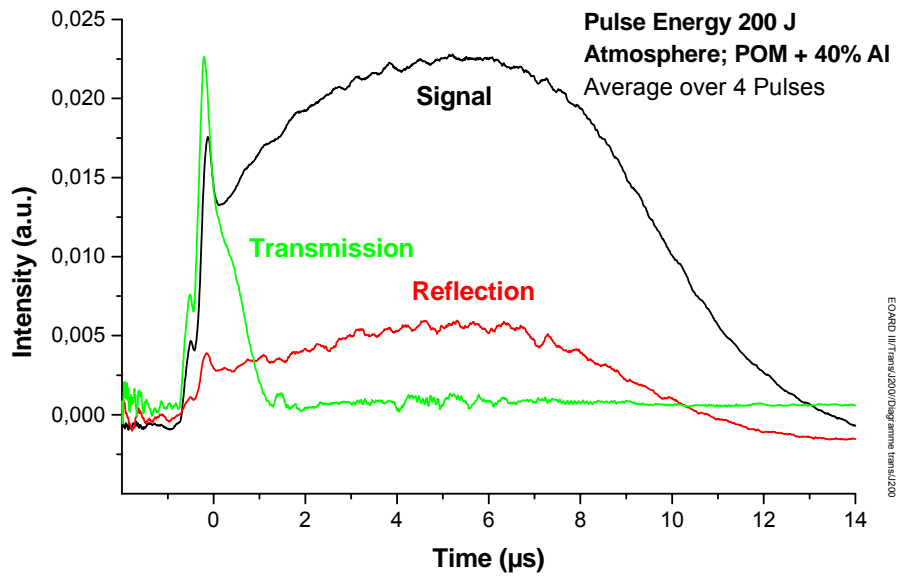
a)



b)



c)



d)

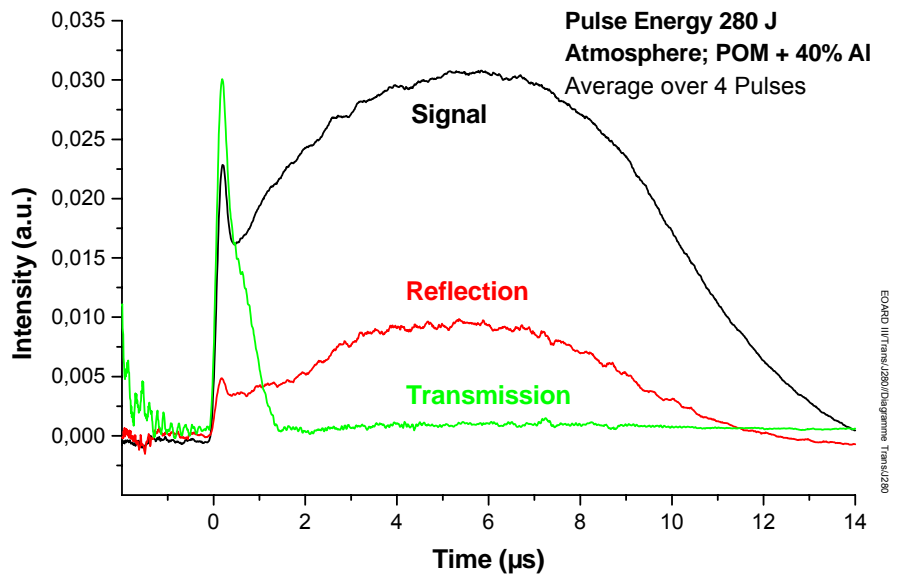


Diagram 31 a-d Time resolved signals of the incident, the reflected and the transmitted laser power for 4 levels of the incident energy. The curves are not of equal scale.

For all energy levels the leading spike of the pulse is present in the transmitted signal. At the lowest value of the pulse energy the power after the spike is considerably reduced compared to the incident power signal and drops steadily towards zero as the pulse continues. At 120 J the transmitted pulse has shortened to about 3 μs and to 1.5 μs at full energy of 280 J. The pulse shortening is graphically displayed in **diagram 32**. By closer inspection of the power curves, it can be seen, that the transmitted power does not fully go to zero. There remains a low level underground that is transmitted during the whole pulse duration.

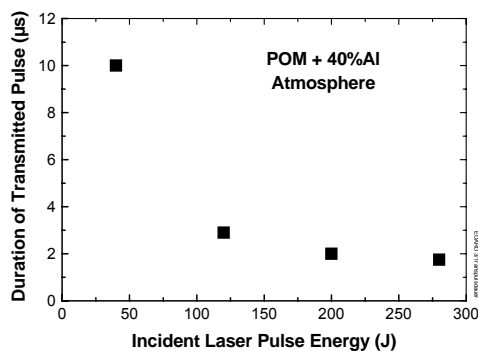


Diagramm 32 Pulse duration shortening effect with incident pulse energy

If the transmitted power can be regarded as the actual power that irradiates the target surface, then both, the pulse shortening and the reduction in magnitude leads to a substantial loss of the effective laser energy. The consequence would be that the given definitions of the coupling coefficient and the deposited energy are doubtful, since they relate the impulse and the mass to the energy

in the laser beam and not to the incident energy on the target surface. In principal, the truly incident energy could be calculated from the ratio of the integrals of the profiles of the transmitted power to the laser power. The problem is to find points in the profile that can be hooked up to each other, so as to have a relative calibration of the signals.

4.6 Tests with doped material in a light concentrating structure

These experiments have been carried out with the standard bell shaped parabolic structure that has been investigated in earlier studies (Ref. 2 and 3). In those experiments Delrin cylinders of 15 mm in length and 8 to 10 mm in diameter had been placed in the focal region of the device as the solid propellant. In the present experiments 4 representative materials were used: POM, POM + 40% Al, Epoxy + 17% Al, and Epoxy + 17% Mg.

Since there was no more sufficient raw material available to produce such cylinders, they have been assembled by stacking together disks with 9.5 mm in diameter, manufactured from the already used flat samples. The new cylinder was 18 mm long. The disks were not solidly bonded to each other. This caused a problem, since in the vicinity of the focal spot the disks were torn apart by the laser pulse, what may have falsified results.

In the following, the results for experiments in the ambient atmosphere will be shown for the four selected probes. Experiments in the vacuum chamber have been attempted as well. However, it turned out that the created impulse was too small or in other words, the concentrating structure was too heavy to allow a measurable displacement. These experiments may be repeated at some later time.

Since all the previous arguments for measurements in air hold here as well, the graphs need not be commented. The pulse energy in all the experiments was 193 J.

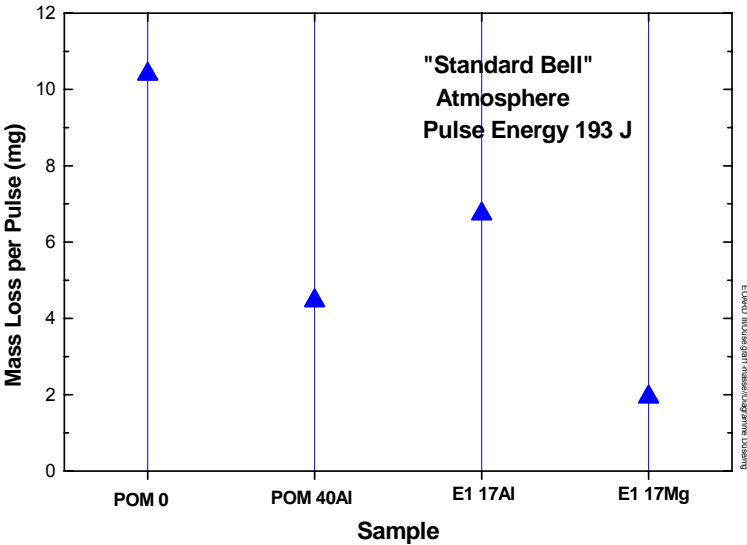


Diagram 33 Mass loss per pulse for 4 samples in the bell nozzle

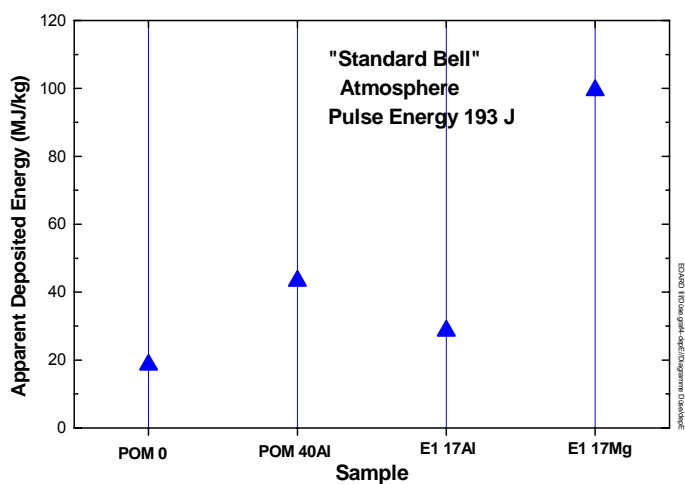


Diagram 34 Apparently deposited energy for 4 samples

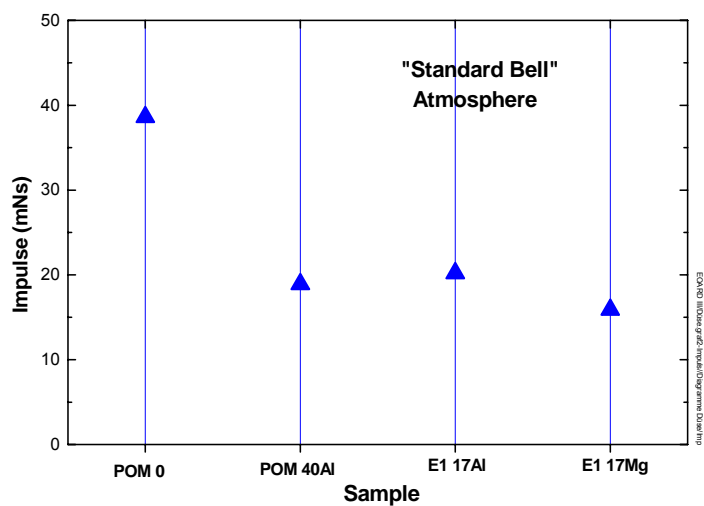


Diagram 35 Measured impulse for 4 samples

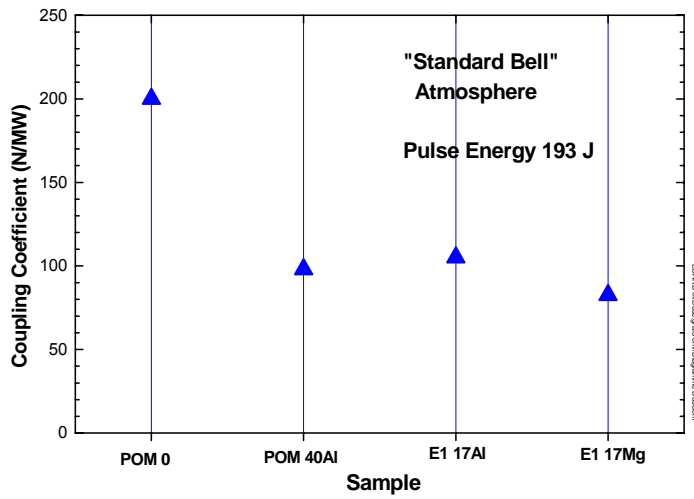


Diagram 36 Coupling Coefficient for 4 samples

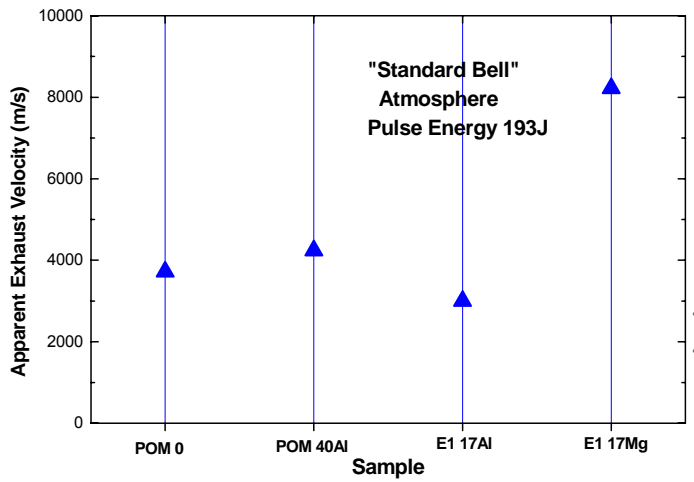


Diagram 37 Apparent exhaust velocity for 4 samples

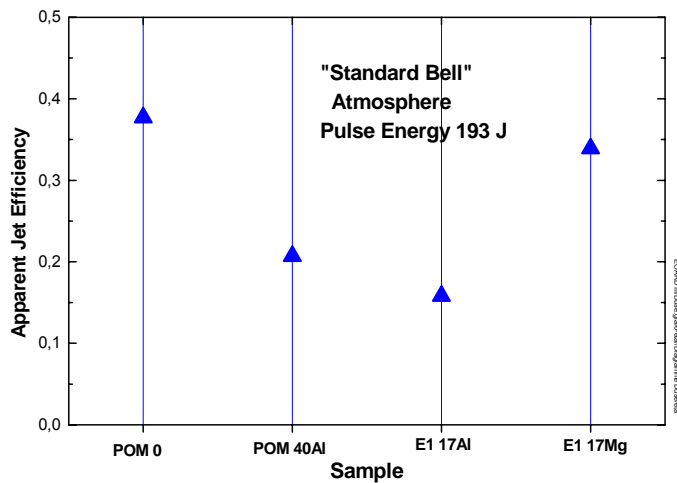


Diagram 38 Apparent Jet efficiency for 4 samples

Regarding the coupling coefficient the value for plain POM with 200 N/MW is roughly in the range of earlier measurements (250 N/MW), so there is some credibility in this number. As in the experiments with the flat samples, the other materials with metal content showed a poorer performance. On the other hand, the ablated mass is also less and particularly so for the Mg doped resin, which shows up in a higher apparent deposited energy and for Mg in an increased apparent exhaust velocity.

4.7 Inspection of the used samples by electron micrography

The pictures of all inspected samples are documented in the picture gallery of Appendix 2 A2. In order to see the effect of the laser pulse on the morphological structure of the material surfaces pictures of two locations are shown: the unaffected edge zone of the probes and the central area of the laser spot.

The first 3 pictures show plain **POM**. At a very high resolution (3000x) flower like spots of unknown origin with radial cracks can be seen. In between there are zones with irregular crack structure. It is believed that the cracks are the consequence of a resolidification of a

molten surface with a contraction of the material due to the rapid cooling. If the edge zone is compared with the central zone at a much lower magnification (100x) it is clearly seen that all the roughness of the surface has been smoothed out by the melting process, leaving only smooth larger “hills” and “valleys”.

Looking with the same magnification at a **POM sample with 20% Al** content, the difference is striking. Although the rough structure, seen at the edge, has also been smoothed out, the surface is grainy. At high resolutions, the grains are identified as the metal grains. However, quite in contrast to the REM pictures of the same surface before the laser pulse the grains are now well rounded. This is also an indication that the grains were heated to the melting point so that the surface tension could smooth out the edges of the grains. A difference may be noticed in the structure of the matrix material POM when compared a probe that was irradiated in atmospherical environment (sample #2) with one irradiated in vacuum (#8). In the case of vacuum the background, from which the grains stand off, appears smoother. Some grains have obviously left the surface and left a crater at their previous location. It is possible that the metal does actually not vaporize and the metal is blown off as a partly solid, partly liquid body. The distribution of the two different materials POM and Al may be seen in the reflecting observation mode for the same sample #8 with 20% Al and for sample #21 with 40% Al.

In high resolution pictures of **POM + 40% Al** (samples #13 in atmosphere and #26 in vacuum) the POM background is only a fraction of the surface and in the vacuum case appears to be retracted.

Finally, one picture is shown with **POM + 60% Al** in the reflecting mode, exhibiting a congregation of nice sphere like metal grains with diameters of a few micrometers up to a maximum of 20 μm .

5. CONCLUSIONS AND RECOMMENDATIONS

The measurements have shown that the expectations to deposit more energy into the metal enriched polymers were not met in any case. The immediate impression of high values for the deposited energy by the lower ablation rate and derived correspondingly high values of the derived jet velocity in air is a pretence caused by a not included and unknown amount of air. This becomes obvious if the ambient pressures is reduced to full vacuum. In this situation the mass dependent quantities become real and show impressively low values.

Trends of decreasing coupling coefficient with increasing energy are an unmistakable sign that the incident energy is absorbed (or reflected) before it arrives at the target. The appearance of absorbing plasma layers (waves) is a well known phenomenon in pulsed or high intensity laser surface interaction. That such phenomena must occur in the presented investigations also has been shown by looking at the energy transmitted through a hole in the sample in comparison to the energy in the laser beam. Also a certain amount of the energy seems to be reflected. The setup for this latter measurement was not ideal because the incident laser beam passed through the same optical element (KCl wedge) as the reflected beam with its orders of magnitude lower intensity. Internal scattering in the wedge from the high intensity laser could have been seen by the detector also. In future experiments of this kind it is recommended to shine the laser beam under a slight angle from the normal on the sample surface. This would not influence the ablation process, but the reflection could be detected without going through the same optics as the high power beam.

The measurement of the transmitted energy gave an idea of how much energy is actually unavailable for the ablation process and is leading to low characteristic numbers that are related to the delivered laser pulse energy. If they could be corrected for the truly incident energy, they would be very much improved. The problem in quantifying the incident

energy on the target surface is the matching of the power scales, that are many orders of magnitude different, for the purpose of relating the two power curves.

This, however, is not a solution to the problem of ablation. To make the full laser energy available for the creation of an impulse requires a complete understanding of the absorption plasma characteristics. These are the speed of development, the extension, and the motion of the plasma wave. Such informations can be obtained by highspped optical methods, looking at the plasma luninescence or, more directly, by absorption measurements transversely to the expansion direction of the absorption wave in a time-of-flight arrangement (at least two probe beams at various distances from the target surface).

One solution may be found in the application of shorter laser pulses, which do not allow sufficient time for the separation of the absorbing cloud from the surface. Since the velocity of the absorption wave is probably somewhat larger than the anticipated material velocity of up to 8000 m/s or 8 mm/ μ s and the wave should not move away farther than a few millimeters during the laser pulse, then the pulse must not be longer than a few hundred nanoseconds. If this assumption is correct a positive effect should already be seen at pulse lengths of a few microseconds. Pulses of a length as short as 2 to 3 μ s should be possible with the available laser.

If the characteristics of the absorption wave are known, new methods may be designed to actually make use of this plasma for the propulsion process proper. Possibilities could be in finding geometries that catch the plasma or in the application of electromagnetic forces.

If the problem of the absorption wave is not solved or at least mediated, it may turn out that the simple concept of laser propulsion might remain inefficient and the required values for the specific impulse and the efficiency may not be reached.

Literature

1. Dennis A. Reilly, "Laser Propulsion Experiments Final Report", AVCO Research Lab, Inc., Everett Maine, 02149, Subcontract B116822 for University of California Lawrence Livermore National Laboratory, Jordan Kare, Program Manager, 1991.
2. W. O. Schall, W. L. Bohn, H.-A. Eckel, W. Mayerhofer, W. Riede, E. Zeyfang, "US – German Lightcraft Impulse Measurements", EOARD Report under contract no. F61775-00-WE033, April 2001.
3. W. O. Schall, H.-A. Eckel and S. Walther, "Lightcraft Impulse Measurements under Vacuum", EOARD Report under contract no. FA8655-02-M4017, September 2002.
4. C. W. Larson, F. B. Mead, Jr., and W. M. Kalliomaa, "Energy Conversion in Laser Propulsion III, Proceedings of High-Power Laser Ablation IV, Taos, NM, 22-26 April 2002, SPIE International Society for Optical Engineering, Vol. 4760, pp. 887-894 (2002).
5. W. O. Schall, W. L. Bohn, H.-A. Eckel, W. Mayerhofer, W. Riede, and E. Zeyfang, "Lightcraft Experiments in Germany", Proceedings of High-Power Laser Ablation III, Santa Fe, NM, 24-28 April 2000, SPIE International Society for Optical Engineering, Vol. 4065, pp. 472-481 (2000).
6. W. O. Schall, H.-A. Eckel, W. Mayerhofer, W. Riede, and E. Zeyfang, "Comparative Lightcraft Impulse Measurements", Proceedings of High-Power Laser Ablation IV, Taos, NM, 22-26 April 2002, SPIE International Society for Optical Engineering, Vol. 4760, pp. 908-917 (2002).
7. W. L. Bohn and W. O. Schall, "Laser Propulsion Activities in Germany", Proceedings of the First International Symposium on Beamed Energy Propulsion, November 5-7, 2002, Huntsville, AL (in press).
8. T. Lippert, J.T. Dickinson, "Chemical and spectroscopic aspects of polymer ablation: Special features and novel directions", Chemical Reviews Vol. 103, No. 2, 2003 p.453-485
9. J.H. Brannon, J.R. Lankard, "Pulsed CO₂ laser etching of polyimide", Appl. Phys. Lett. Vol. 48, No. 18, 5. May 1986, p.1226-1228.
10. M.F. Sonnenschein, C.M. Roland, "High-resolution ablation of amorphous polymers using CO₂ laser irradiation", Appl. Phys. Lett. Vol. 57, No. 5, 30 July 1990, p.425-427.
11. R. Srinivasan, B. Braren, R.W. Dreyfus, "Ultraviolet laser ablation of polyimide films", J. Appl. Phys. vol. 61, No.1, 1. January 1987, p. 372-376.

12. R. Braun, R. Nowak, P. Hess, H. Oetzmann, C. Schmidt, "Photoablation of polyimide with IR and UV laser radiation", *Appl. Surf. Sci.* Vol.43, 1989, p. 352-357.
13. A. Slocombe, L. Li, "Laser ablation machining of metal/polymer composite materials", *Appl. Surf. Sci.* Vol.154-155, 2000, p. 617-621.
14. A. Slocombe, A. Taufik, L. Li, "Diode laser ablation machining of 316L stainless steel powder/polymer composite material. Effect of powder geometry". *Appl. Surf. Sci.* Vol.168, 2000, p. 17-20.
15. D.K.Y. Low, M.J.J. Schmidt, L. Li, "Spectroscopic characteristics of the plume generated during laser ablation of a ceramic-polymer composite", *Appl. Surf. Sci.* Vol.168, 2000, p. 170-174.

Appendix 1 Lightcraft sample list

Sample No.	Designation	Origin	Trade Name	Polymer	Metal	Concentration
1	P-AI0	IPT		POM Ultraform S 23 30 03	-	0
2	P-AI20	IPT		POM Ultraform S 23 30 03	Aluminum	20%
3	P-AI40	IPT		POM Ultraform S 23 30 03	Aluminum	40%
4	P-AI60	IPT		POM Ultraform S 23 30 03	Aluminum	60%
5	B-AI	DLR-RA		Polybutadien	Aluminum	?
6	E2-AI	DLR-BK		Resin F200 + Hardener F250	Aluminium	?
7	E1	DLR-BK		Resin F200 + Hardener F250	-	
8	E1-AI3	DLR-BK		Resin F200 + Hardener F250	Aluminum	3%
9	E1-AI5	DLR-BK		Resin F200 + Hardener F250	Aluminum	5%
10	E1-AI10	DLR-BK		Resin F200 + Hardener F250	Aluminum	10%
11	E1-AI17	DLR-BK + Metal		Resin F200 + Hardener F250	Aluminum	16.6%
12	E1-AI30	DLR-BK + Metal		Resin F200 + Hardener F250	Aluminum	30%
13	E1-AI40	DLR-BK + Metal		Resin F200 + Hardener F250	Aluminum	40%
14	E1-AI50	DLR-BK + Metal		Resin F200 + Hardener F250	Aluminum	50%
15	E1-Mg3	DLR-BK + Metal		Resin F200 + Hardener F250	Magnesium	3%
16	E1-Mg5	DLR-BK + Metal		Resin F200 + Hardener F250	Magnesium	5%
17	E1-Mg10	DLR-BK + Metal		Resin F200 + Hardener F250	Magnesium	10%
18	E1-Mg17	DLR-BK + Metal		Resin F200 + Hardener F250	Magnesium	16.6%
19	E1-Mg30	DLR-BK + Metal		Resin F200 + Hardener F250	Magnesium	30%
20	E1-Mg40	DLR-BK + Metal		Resin F200 + Hardener F250	Magnesium	40%
21	P-Fe	BASF	Catamold ® FS	Polyacetal	Iron	50-70%
22	P-Ti	BASF	Catamold ® Ti	Polyacetal	Titanium	ca. 86%

Abbreviations:
 IPT: Institute for Polymer Technology, Wismar
 DLR-RA: DLR-Institut für Raumfahrtantrieb (Space Propulsion)
 DLR-BK: DLR-Institut für Bauweisen und Konstruktionsforschung
 Metal: Alfa Aesar, Johnson&Matthey Deutschland, Karlsruhe

Appendix 2

GALLERY OF REM PICTURES

Percentages of dopants are given in weight percent. If the content is not given, it is company confidential and thus not disclosed to us.

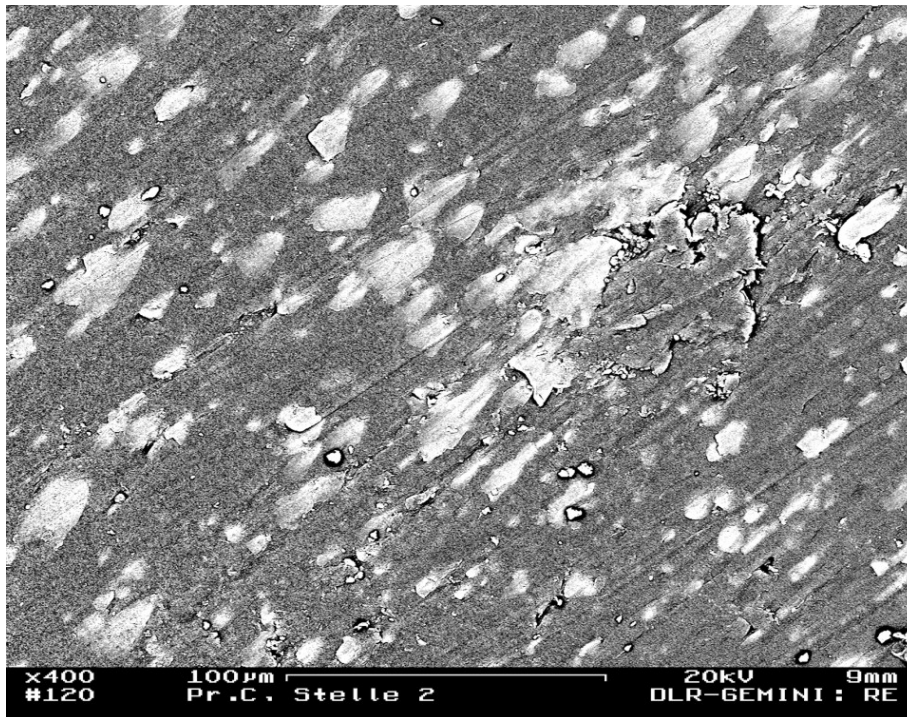
Al Pictures before Laser Treatment

The pictures show representative exposures of all samples up to no. 16 in the same order, as in the diagrams where their ablation properties are compared. The scale in the pictures varies, but is given in the bottom line. A few pictures are contrast enhanced. All pictures are made in the reflective mode to discriminate the different materials.

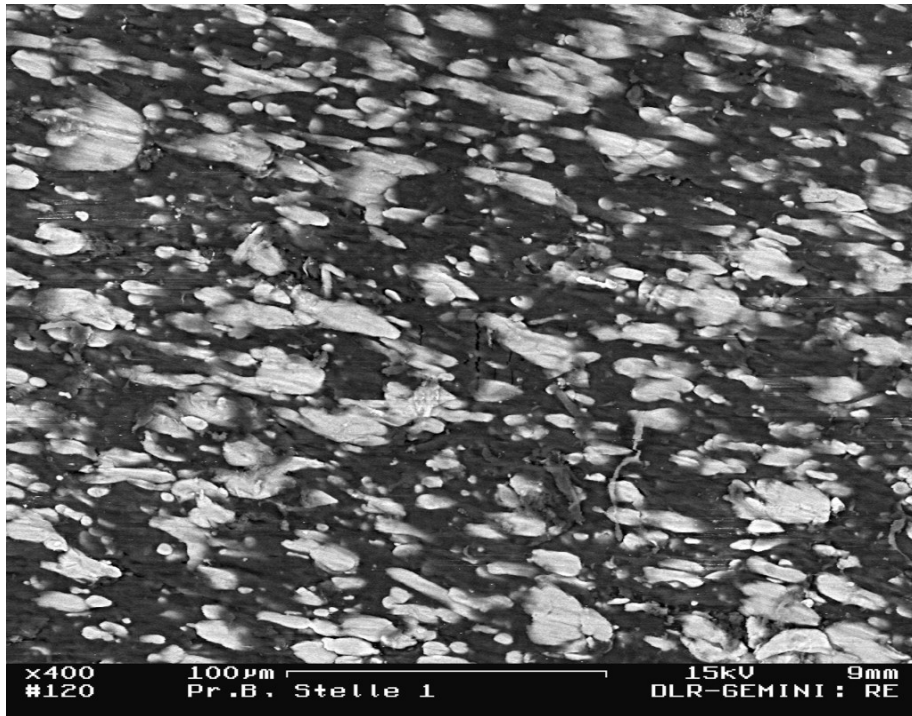
1. POM

No picture is available, because without a difference in materials nothing can be seen in the reflective mode.

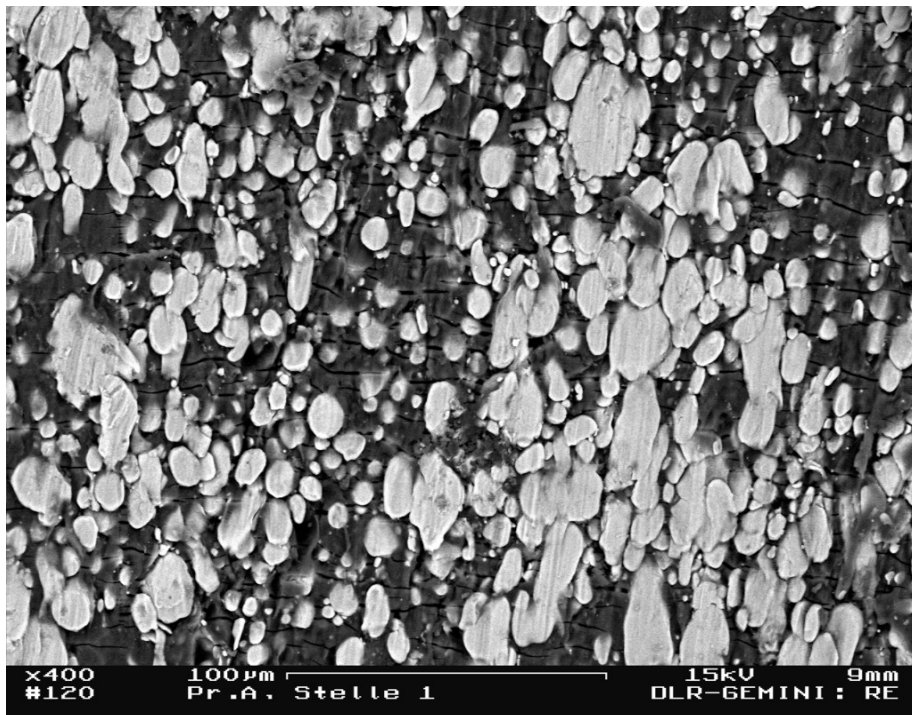
2. POM + 20% Al Sample type 2



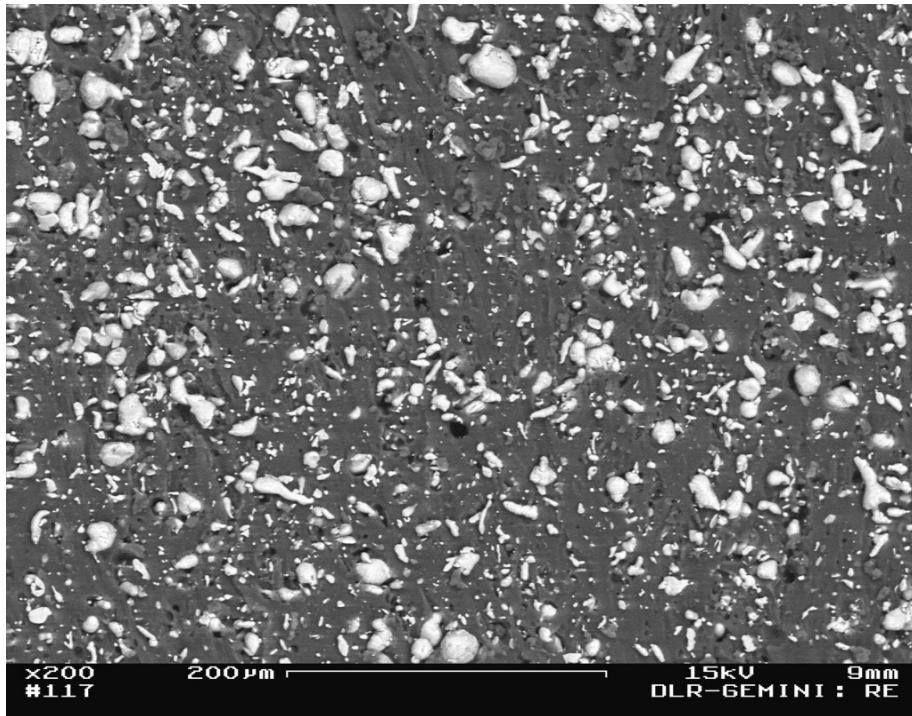
3. POM + 40% Al Sample type 3



4. POM + 60% Al Sample type 4



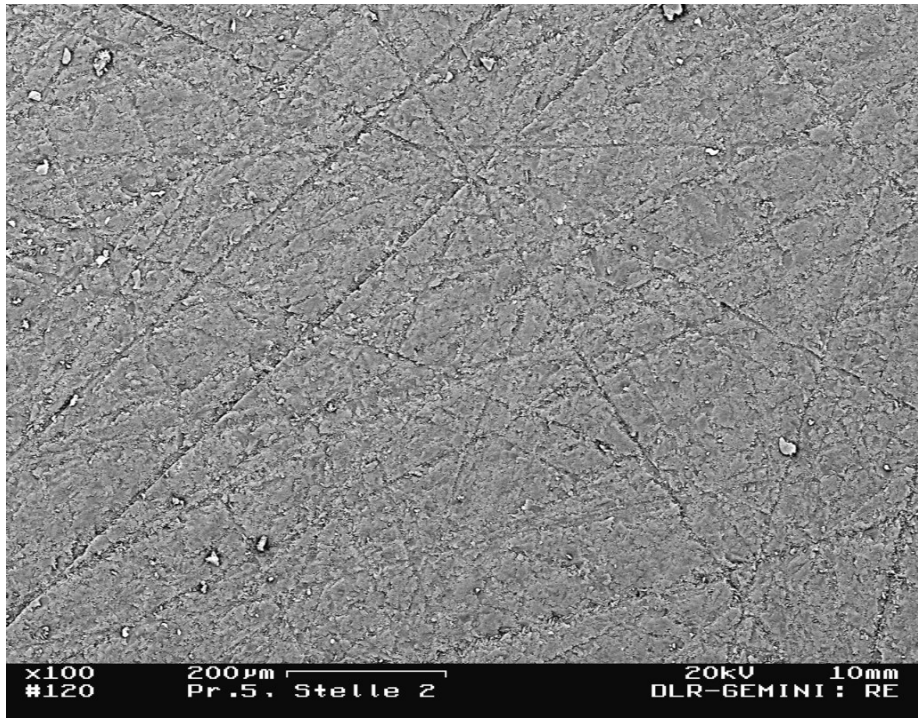
5. Polybutadien + Al Sample type 5



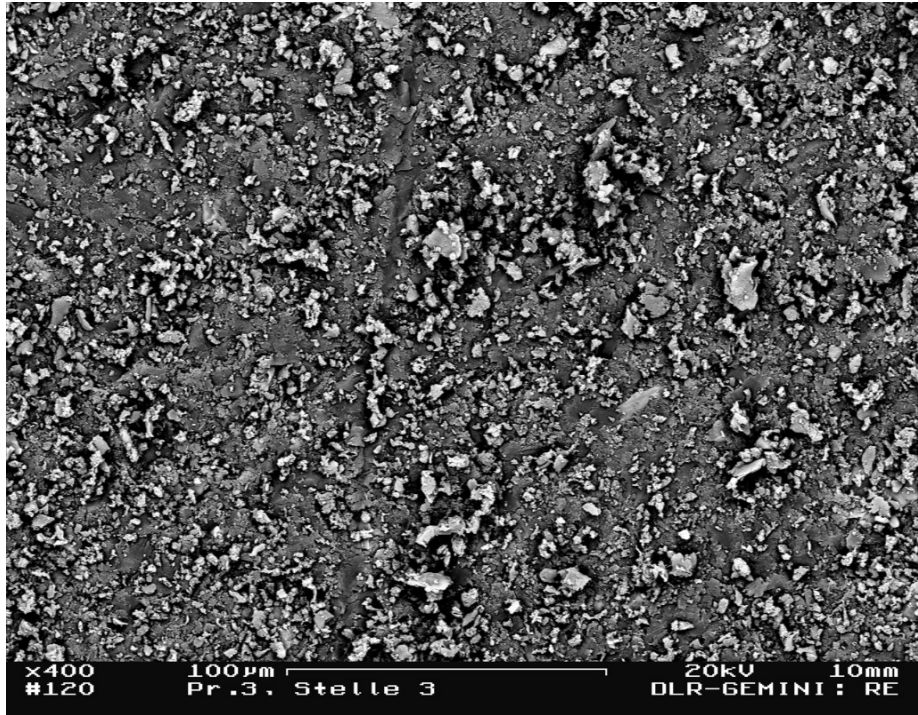
6. Epoxy resin + Al Sample type 6



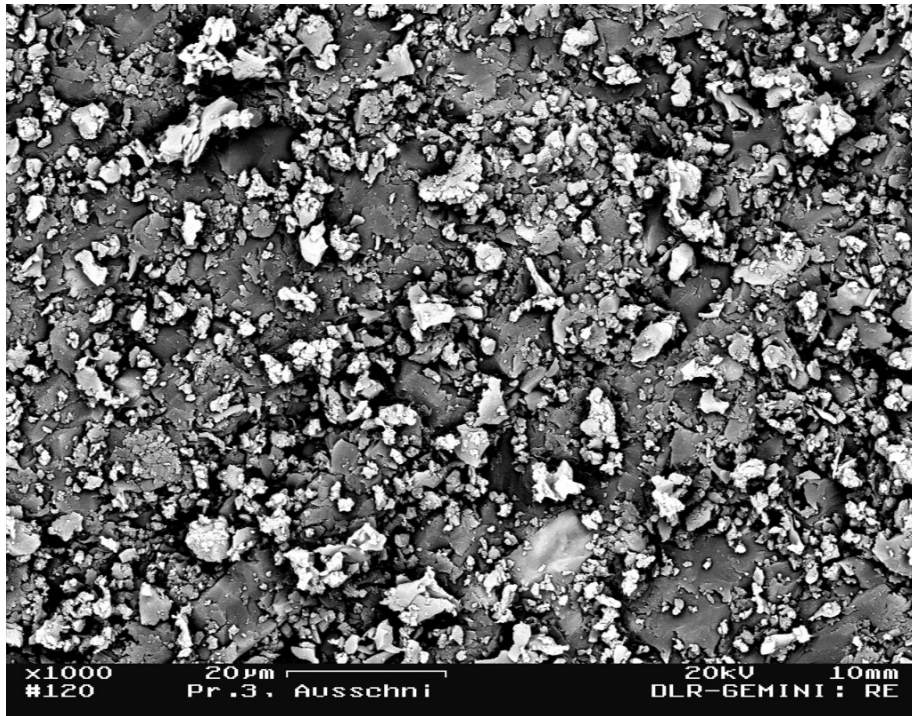
7. Epoxy resin Sample type 7



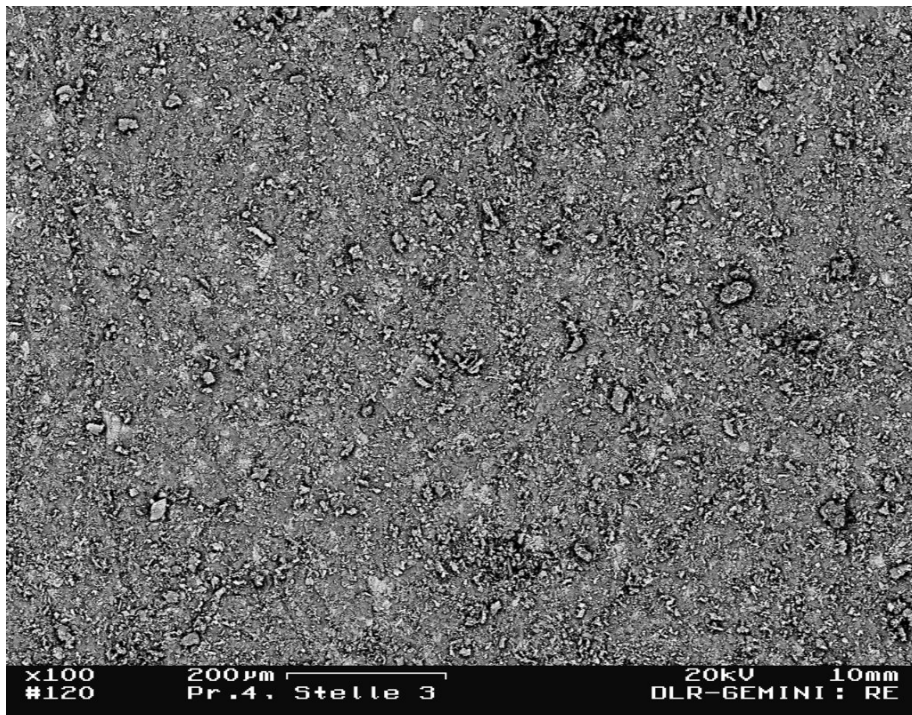
8a. Epoxy + 17% Al Sample type II



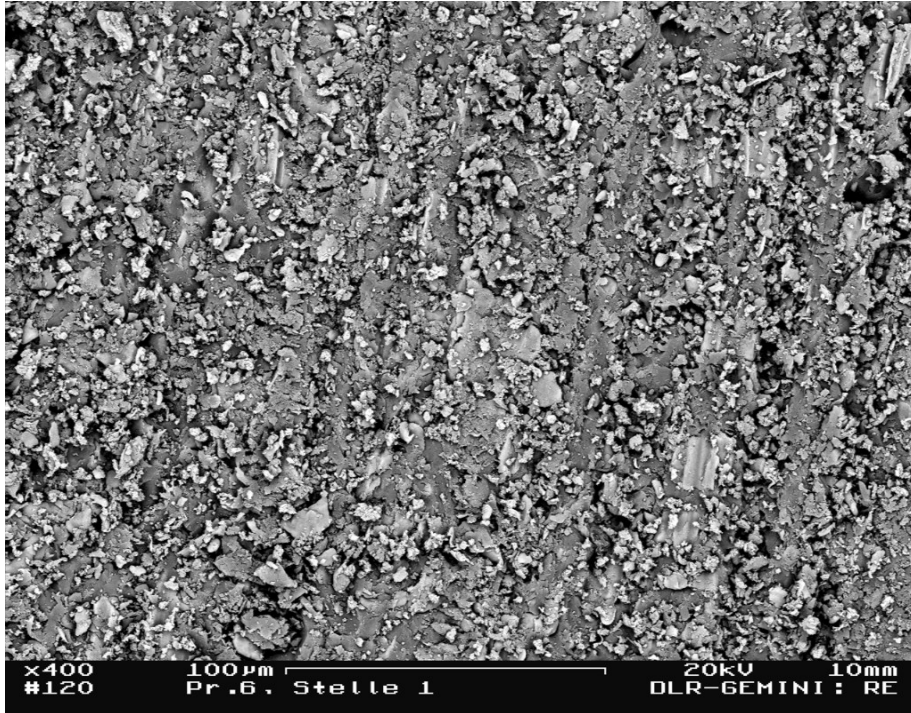
8b. Epoxy + 17% Al (close-up)



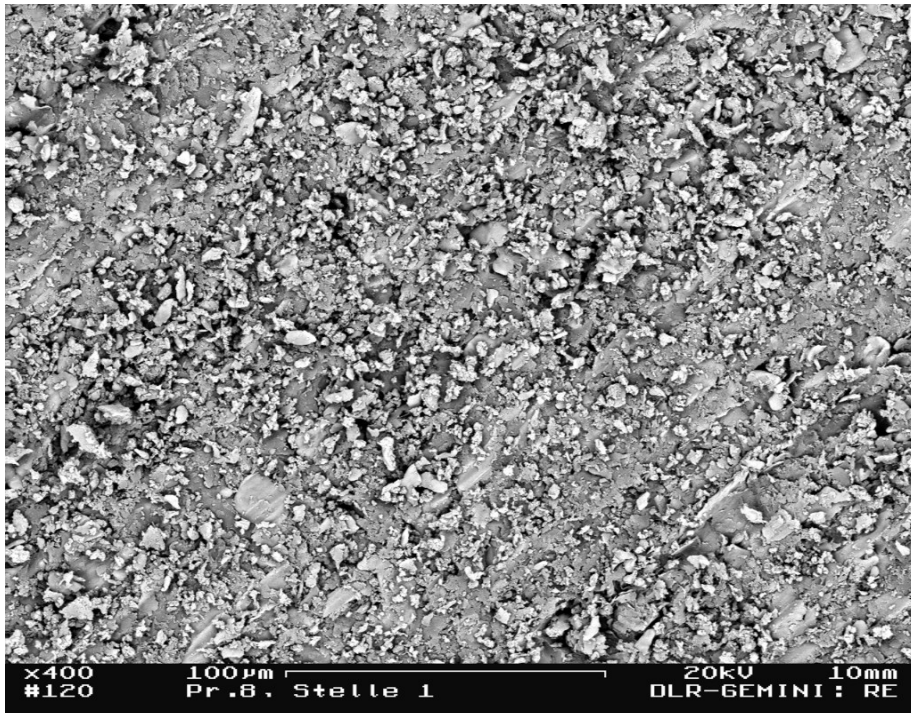
9. Epoxy + 30% Al Sample type 12



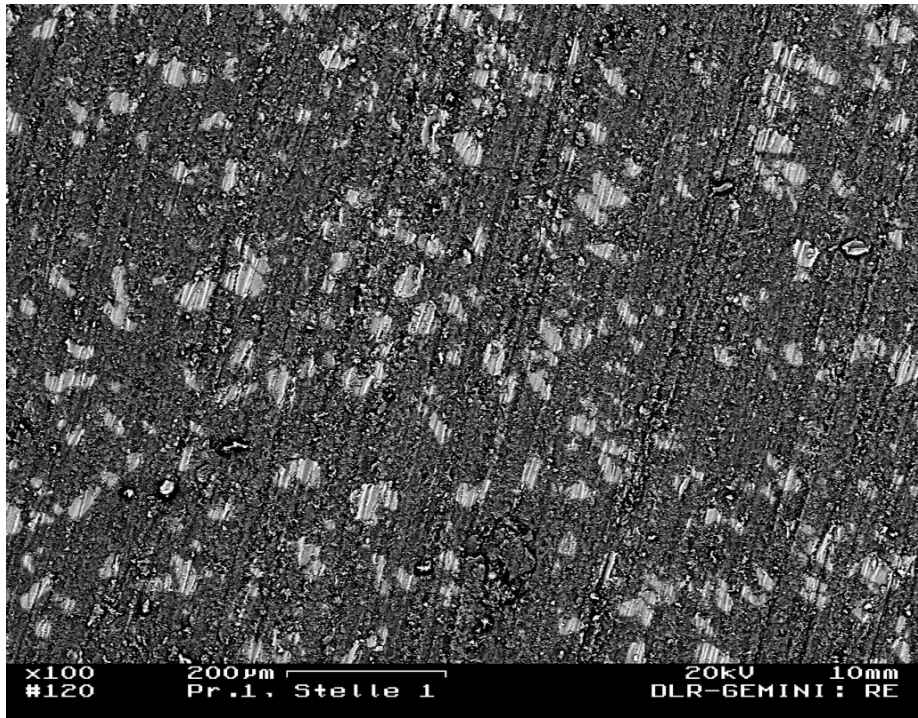
10. Epoxy + 40% Al Sample type 13



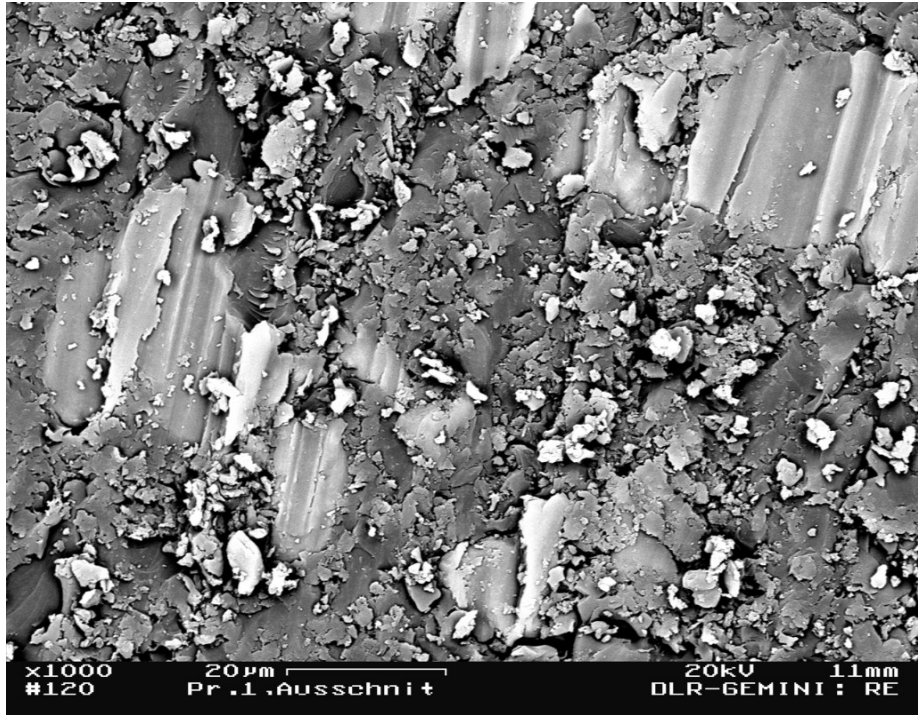
11. Epoxy + 50% Al Sample type 14



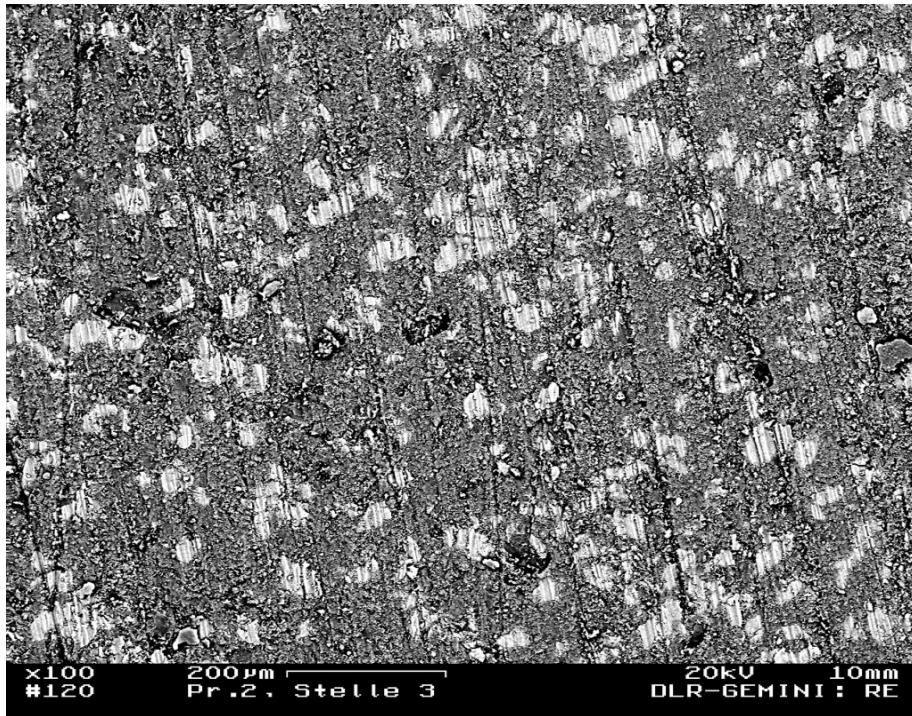
12a. Epoxy + 17% Mg Sample type 18



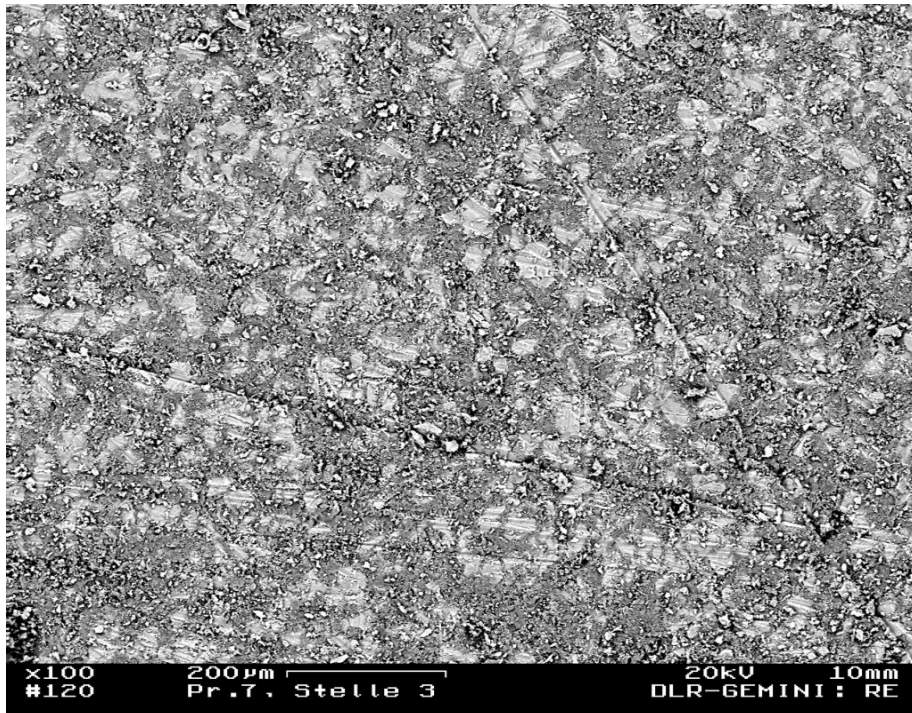
12b. Epoxy + 17% Mg (close-up)



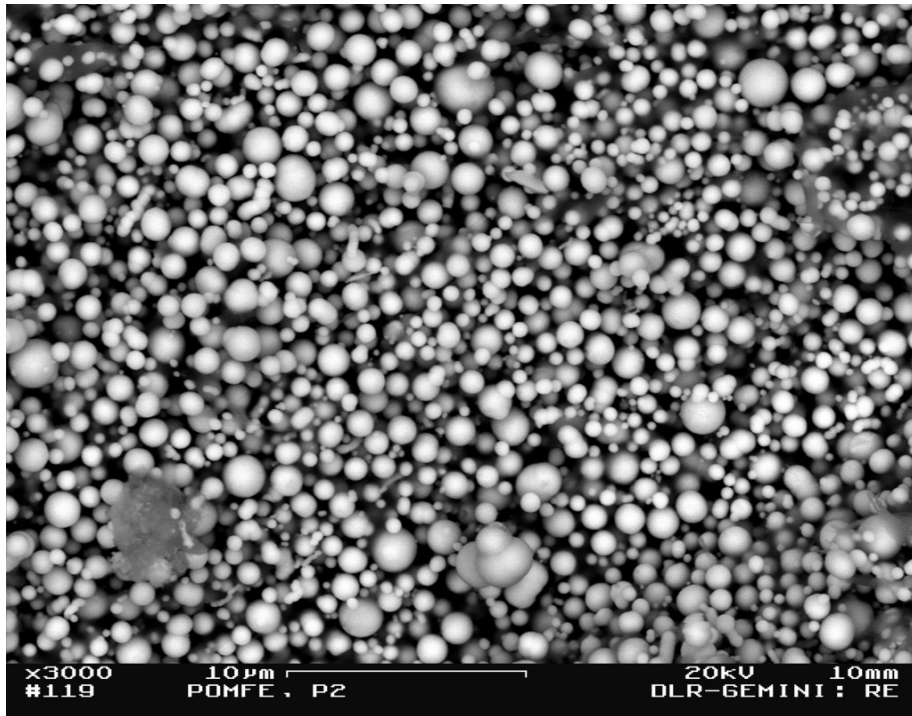
13. Epoxy + 30% Mg Sample type 19



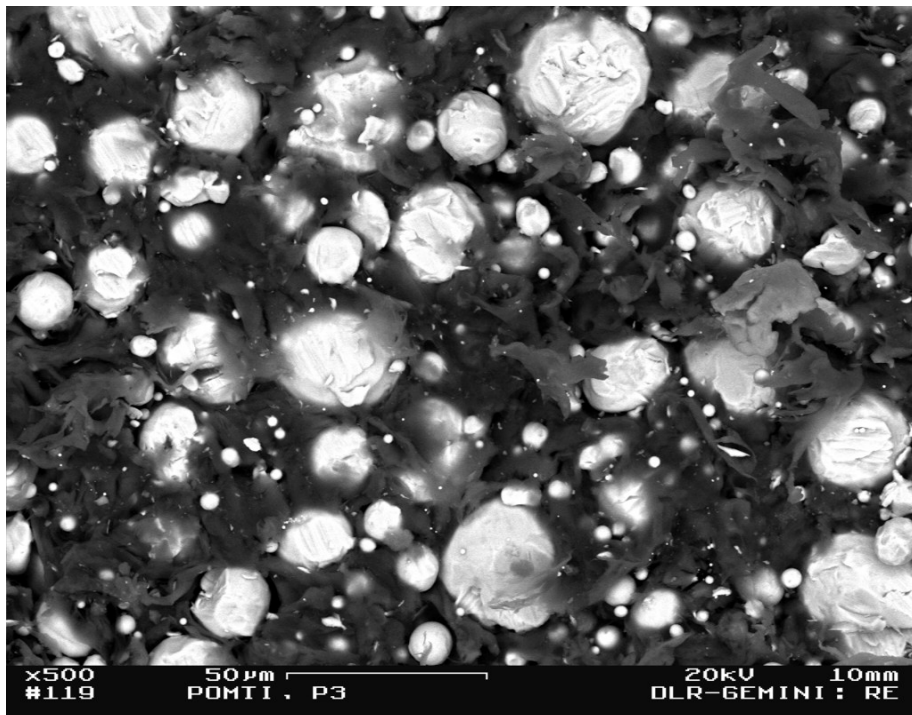
14. Epoxy + 40% Mg Sample type 20



15. POM + Fe Sample type 21



16. POM + Ti Sample type 22



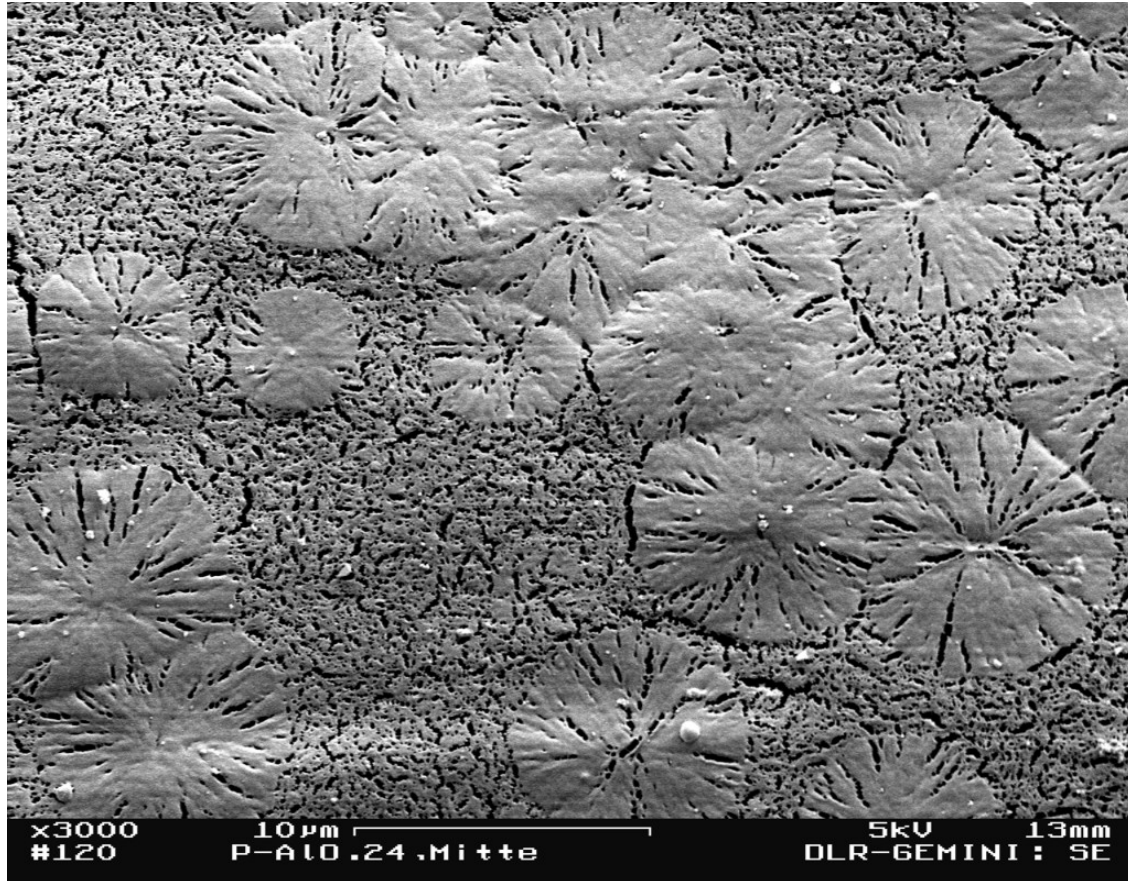
A2 Pictures after Laser Irradiation

Pictures are made only for the baseline samples of POM without and with aluminum dopants in the 3 concentrations of 20%, 40% and 60%. Unfortunately, during the preparation process for the microscopy some samples have been destroyed and no pictures are available. However, it turned out with new samples that indicative differences are not expected to be seen. The probes have been looked at in the reflective mode (RE mode) again, but also in the mode of secondary electron emission (SE mode). In this mode it is possible to see the surface morphology. In particular, it is of interest to see how much of the polymer material has been ablated between the metal grains and if they have undergone a phase transition. The application of the SE mode makes it necessary to sputter the probes with gold or carbon and a distinction of different materials is not possible anymore. Different enlargements have been used to distinguish general surface structures from the immediate vicinity of the Al grains. Furthermore, in some cases photographs of the untreated edge region are compared with the laser irradiated sample center. Also some comparable pictures are provided for ablation in ambient air and in vacuum.

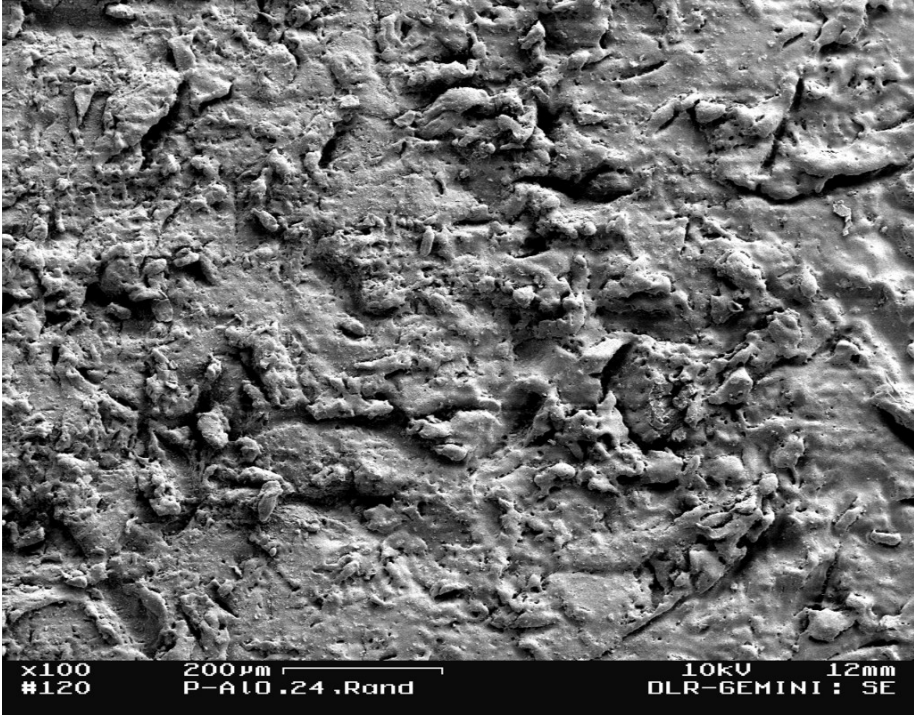
The pictures are discussed in the main text in Chapter 4.7. Here, only the picture parameters are given. Note: The enlargement is indicated in the bottom line of each photograph to the left. Experimental conditions are given in the headline of each picture.

1. POM

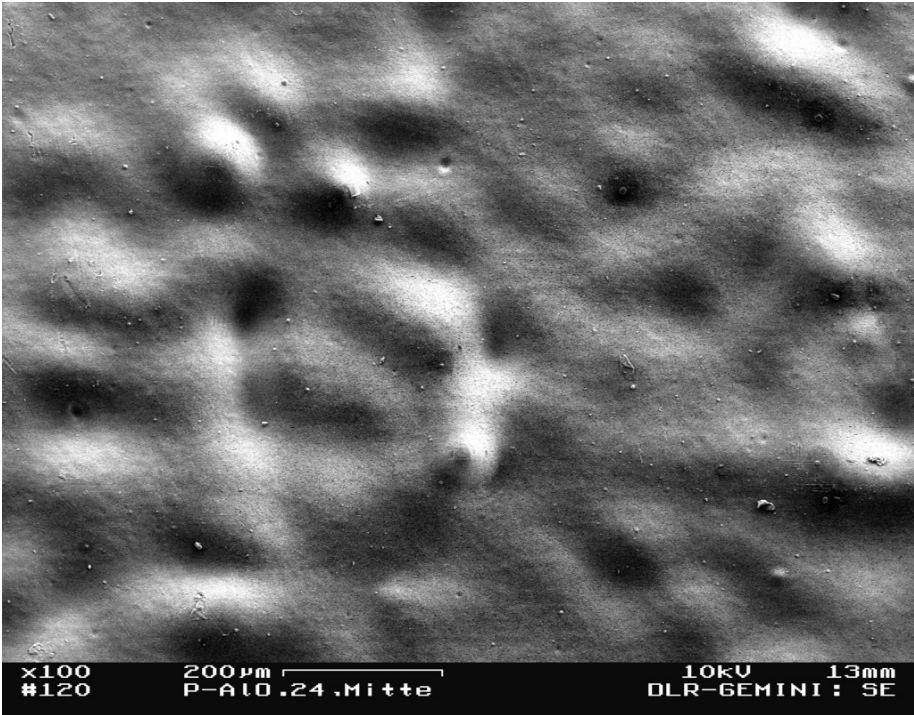
Sample #24; Center; SE-mode; 4 pulses at 280 J; ambient pressure 1000 mbar.



Sample #24; Edge; SE mode

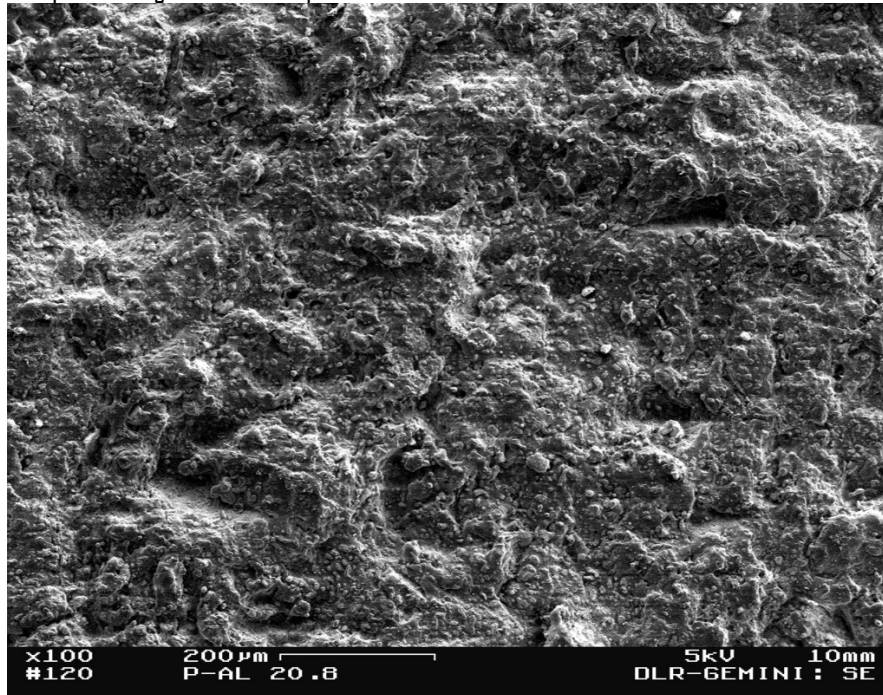


Sample #24; Center; SE mode

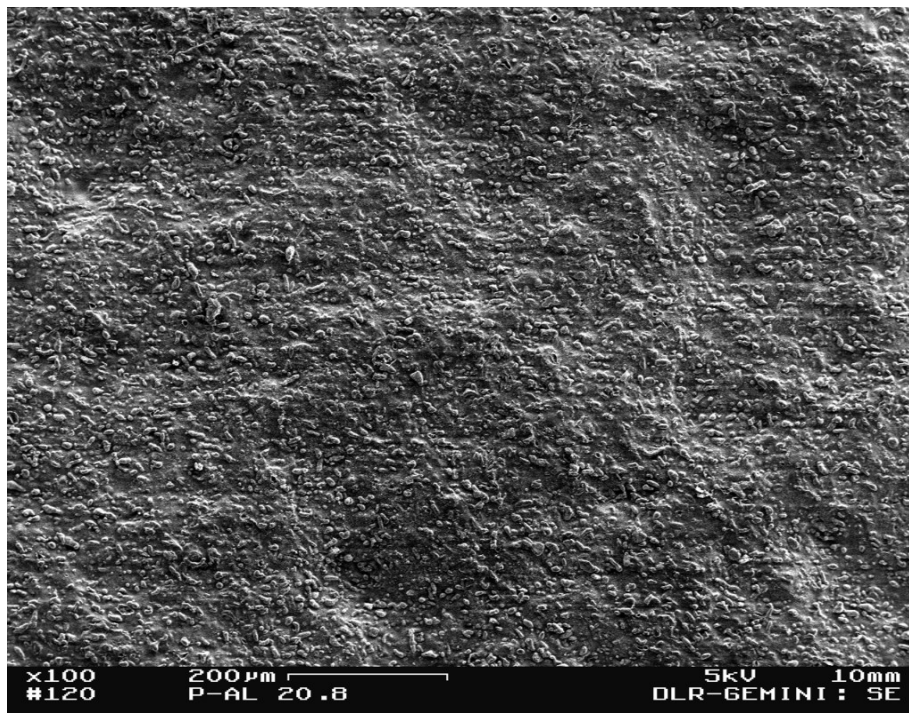


2. POM + 20% Al

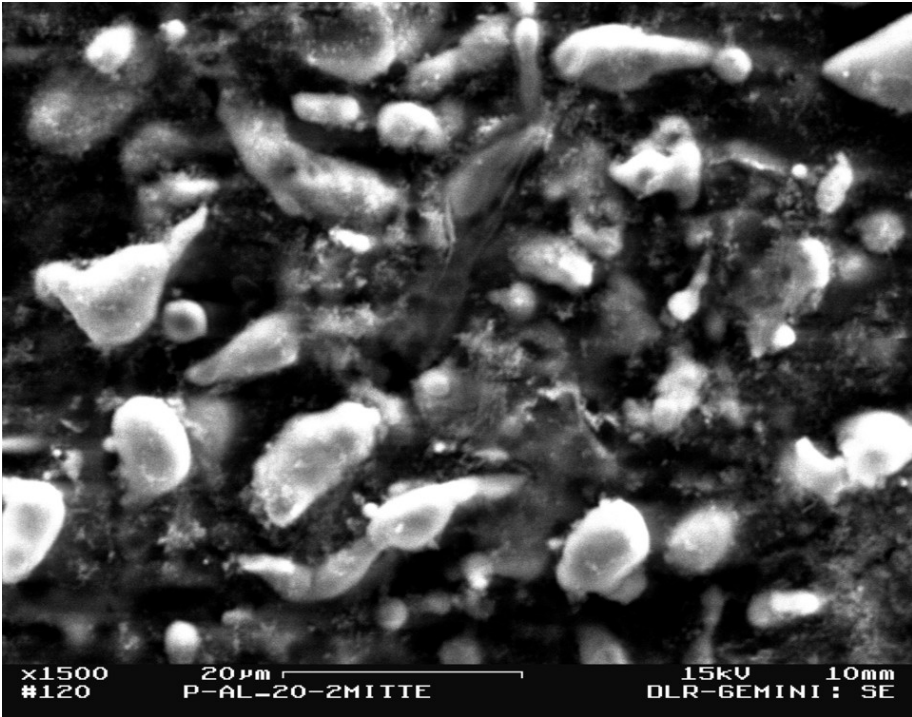
Sample #8; Edge; SE mode; 5 pulses of 200 J; vacuum



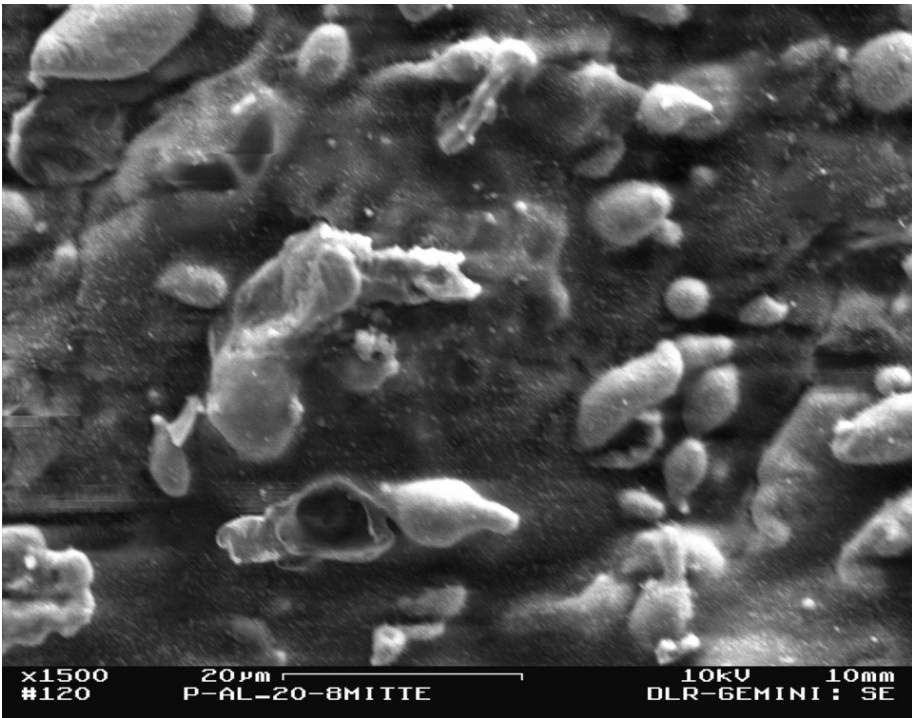
Sample #8; Center; SE mode



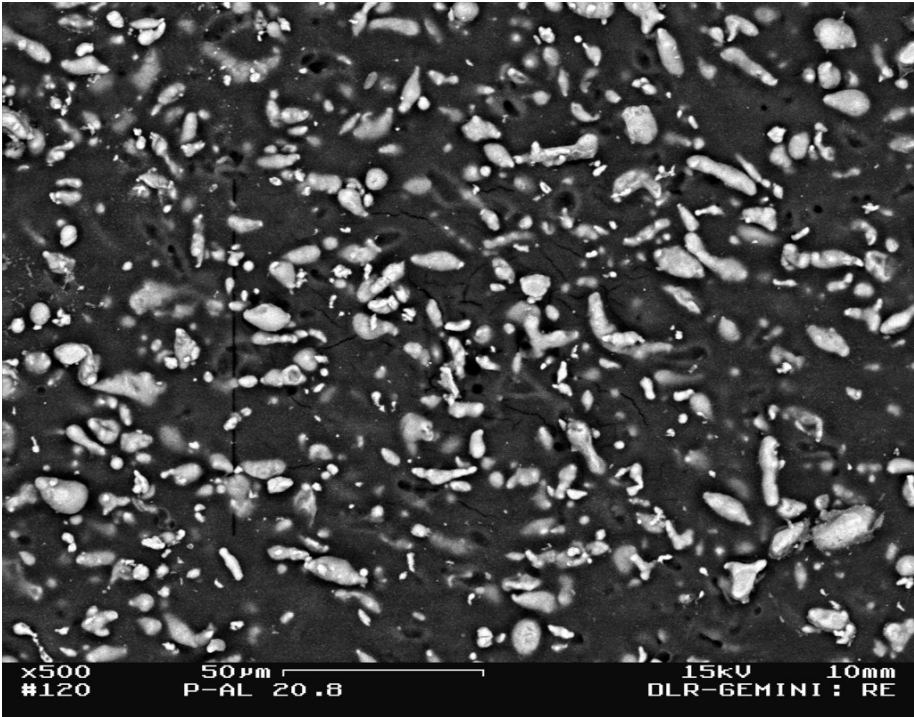
Sample #2; Center; SE mode; 5 pulses at 280 J; 800 mbar



Sample #8; Center; SE mode; 5 pulses at 200 J; vacuum

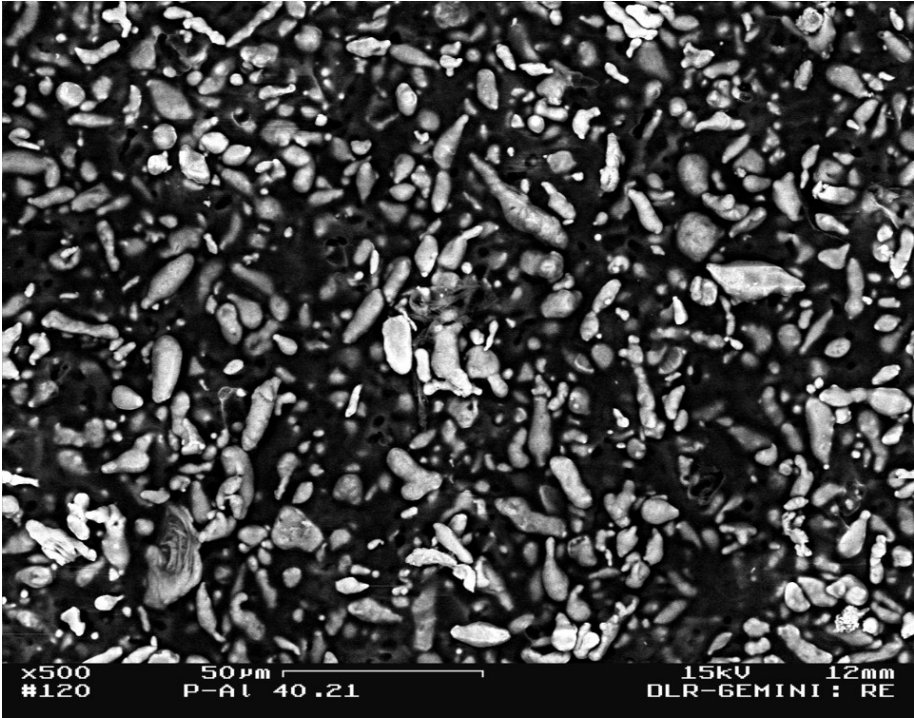


Sample #8; Center; RE mode; 5 pulses at 200 J; vacuum

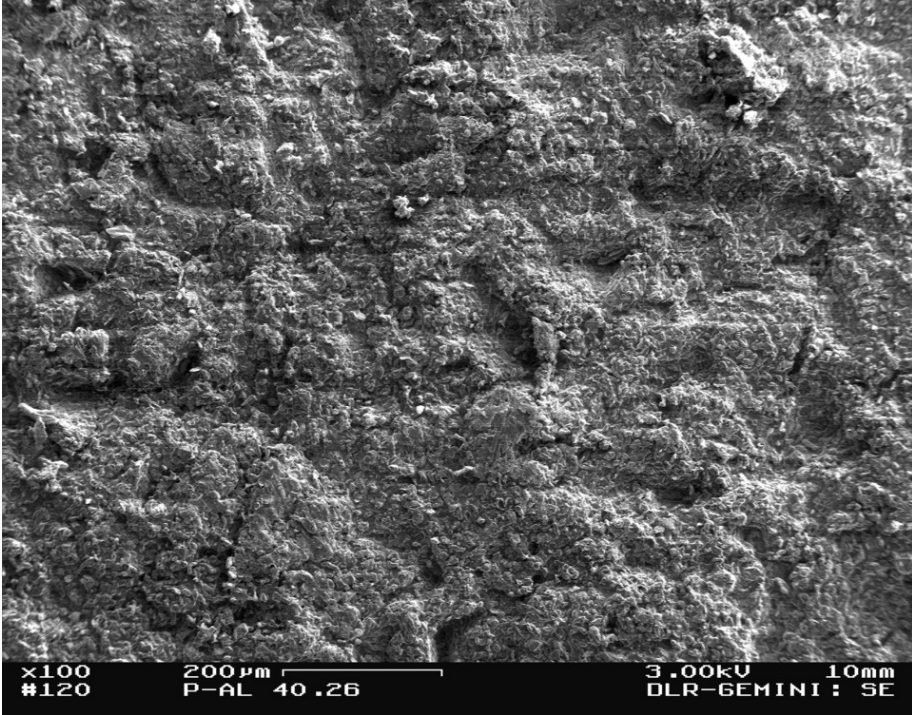


3. POM + 40% Al

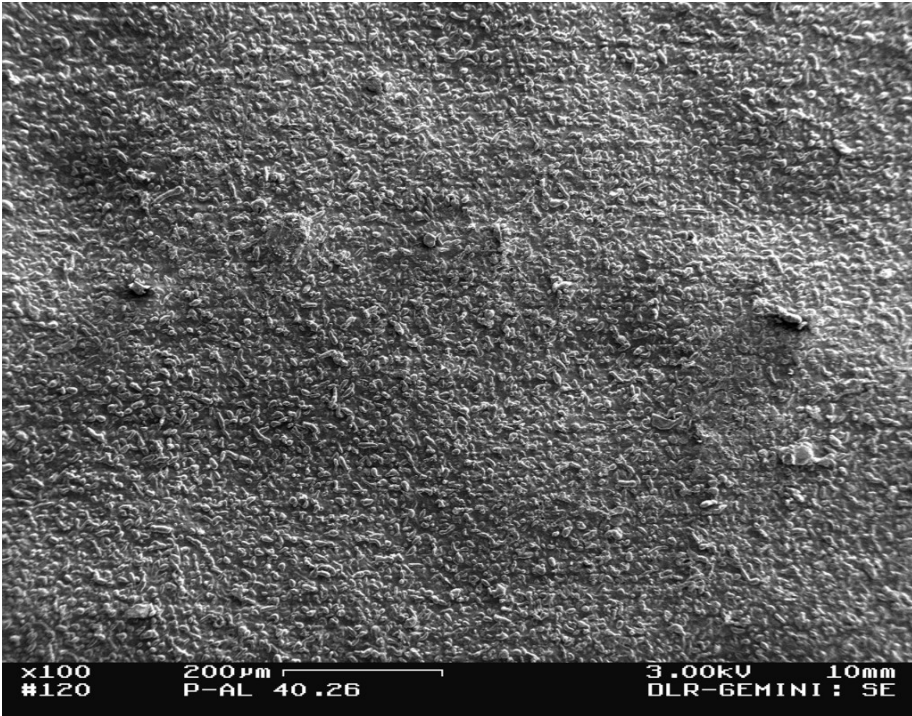
Sample #21; Center; RE mode; 5 pulses at 120 J; vacuum



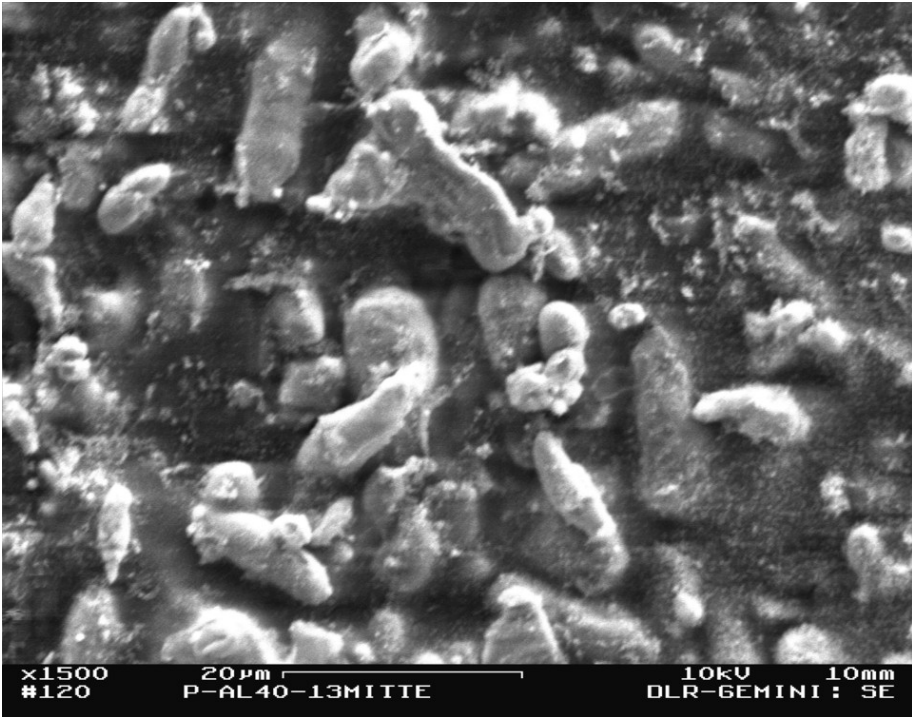
Sample #26; Edge; SE mode; 5 pulses at 200 J; vakuum



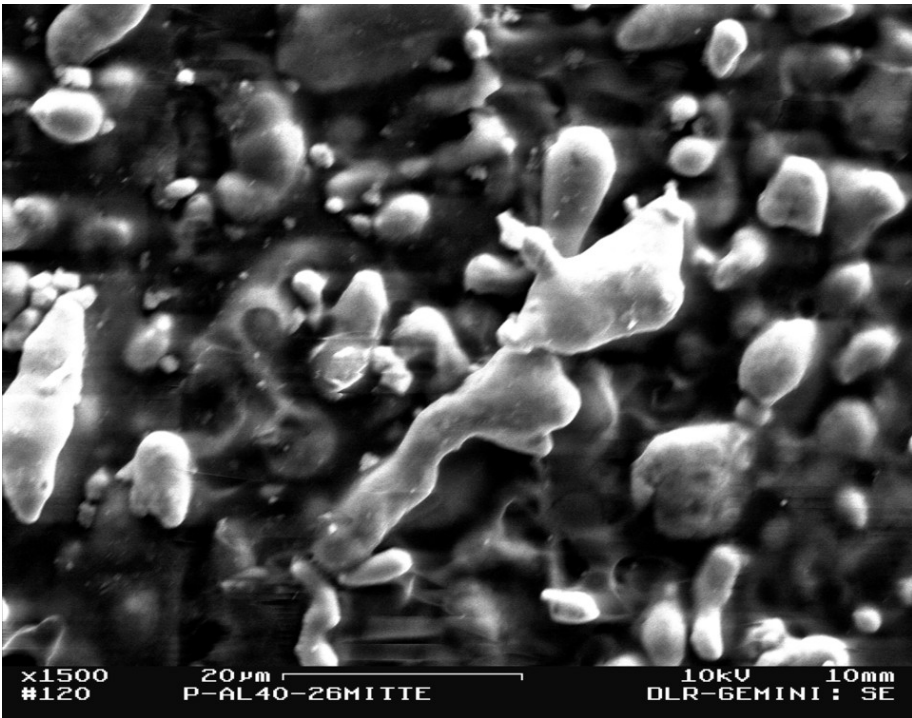
Sample #40; Center; SE mode; 5 pulses at 200 J; vakuum



Sample #13; Center; SE mode; 5 pulses at 200 J; 1000 mbar



Sample #26; Center; SE mode; 5 pulses at 200 J; vacuum



4. POM + 60% Al

Sample #7; Center; RE mode; 5 pulses at 200 J; 1000 mbar

